Local Structures of AgxCu1-xI by means of NMR, ab initio MO and MD methods

メタデータ	言語: eng
	出版者:
	公開日: 2017-10-05
	キーワード (Ja):
	キーワード (En):
	作成者:
	メールアドレス:
	所属:
URL	http://hdl.handle.net/2297/30603

学位論文

Local Structures of $Ag_XCu_{1-X}I$ by means of NMR, ab initio MO and MD methods

NMR、分子軌道法および分子動力学法による

$Ag_XCu_{1-X}I$ の局所構造解析

Tomonori Ida

井田　朋智

March, 2001

Division of Basic Science,

Graduate School of Natural Science and Technology,

Kanazawa University, Kanazawa, Japan

Doctor Thesis

Local Structures of $Ag_X Cu_{1-X} I$

by means of NMR, ab initio MO and MD methods

By

Tomonori Ida

March, 2001

Division of Basic Science,

Graduate School of Natural Science and Technology

Kanazawa University

Kanazawa, 920-1192, Japan

Acknowledgment

Contents

Chapter 1

Introduction

About thirty years ago a new interest arose in studying solids with high ionic conductivity. These materials were termed "solid electrolytes" or "superionic conductors" (SIC) and this new field of interdisciplinary research became known as Solid State Ionics. Among the many topics of practical applications of superionic conductors one should mention fuel cells, energy storage and conversion (e.g. Na/S batteries), chemical sensors and electrochromic displays. Parallel to this, the fundamental aspects of fast ionic motion in solids became a very active research field. In some areas, it was the new interest in solid electrolytes, which triggered a fresh look at classical problems such as diffusion, and its correlated effects in solids.

The ionic conductivity of a SIC is comparable to that of liquid electrolytes. There is no sharp distinction between these solids and those, like NaCl, which show "normal" conduction. However, solids, which are characterized by an ionic conductivity larger than 10 S/m and low activation energy of the order of 10kJ/mol, fall into the domain of Solid State Ionics.

Fast ion conduction takes place in a variety of substances such as crystals, glasses and

polymers. Ionic conduction or diffusion in solids requires the presence of some disorder or defects. Due to thermal vibrations the ions sometimes receive enough energy for them to be pushed to a nearby vacant lattice site or into an interstitial site: this leads to diffusion. According to Ratner and Nitzan [1], we divide solid electrolytes into two groups: hard and soft framework crystals. The soft crystals, like AgI, CuI, Ag_2HgI_4, are characterized as follows: (i) the bonding is high ionicity; (ii) the mobile ions are, generally, polarizable and heavy (Ag, Cu); (iii) the Debye temperatures are low; (iv) a sharp order-disorder phase transition exists between the low and high conducting phase accompanied by a large increase of the enthalpy.

On the other hand, hard framework crystals are usually oxides (e.g. β-alumina, $LiAlSiO_4$, hollandite) and are characterized by covalent bonds. Consequently they have high frequencies for local vibrations, high Debye temperature, low polarizability of the mobile ions and generally do not exhibit the ionic phase transition.

In this study, we are concerned with the AgI crystal and doped one with CuI which are a typical soft framework SIC. The crystals have the zincblende structure (γ-phase) below the superionic phase transition point, while the substance changes to the superionic phase (α-phase) at high temperature. In the α-phase, the iodine sublattice possesses a body-centered cubic arrangement as shown in Fig.1.1, with the Ag atom located in distorted tetrahedral 12(d) sites and with some amount of densities at trigonal 24(h) and octahedral 6(b) positions, as obtained from a neutron diffraction study [2]. Boyce and co-worker indicated that the distribution of the Ag atom slightly displaces from the center of the 12(d) sites, by considering an extended X-ray absorption fine structure [3]. In more recent papers [4-6], McGreevy and co-workers showed the local density and pathway for the diffusion of the silver ion from the neutron powder diffraction analysis. Although numbers of investigators have been very interested in

determining the average structures of the silver ion in the α-AgI by the X-ray and neutron diffraction methods, we think that the dynamical motion of the cations is much important in the superionic conductor.

Molecular dynamics (MD) method is a powerful tool of the theoretical approach to the dynamical structural analysis of liquid and crystal. In the early time of development of the MD method, it was applied by Schommers [7,8] and by Vashishta and Rahman [9] to investigate α-AgI. The latter authors succeeded to describe the stability of the anion sublattice and the density distribution of cations as well as the diffusive motion of cations by assuming a rather complicated ionic potential. It is, however, not easy to understand which part of the potential is responsible for the stability of the anion sublattice and/or for the large diffusive motion of cations.

A more simple and natural extension of the soft-core system to ionic systems may be to assume that an interionic potential consists of two parts, that is, a soft-core repulsion and a Coulombic term. This type of ionic potentials were applied by Hansen and McDonald to study a molten salt [10] and by Amini, Finchman and Hockney to investigate the melting of alkali halide crystals [11]. For α-AgI, Fukumoto, Ueda and Hiwatari investigated this extended version of the soft-core system as a model [12]. The work clarified the salient relationship between the interionic potentials and the characteristic features of SIC. Other some groups applied this potential to obtain the microscopic information for α-AgI [13-15]. The MD simulations surely explained the dynamical information for α-AgI in detail, no studies have ever been tried to apply the MD method to NMR spectral analysis which gave much detailed microscopic local informations selectively.

Solid-state nuclear magnetic resonance (NMR) is a powerful tool to examine the dynamic and static structure of crystal. NMR has played an important role in solid state
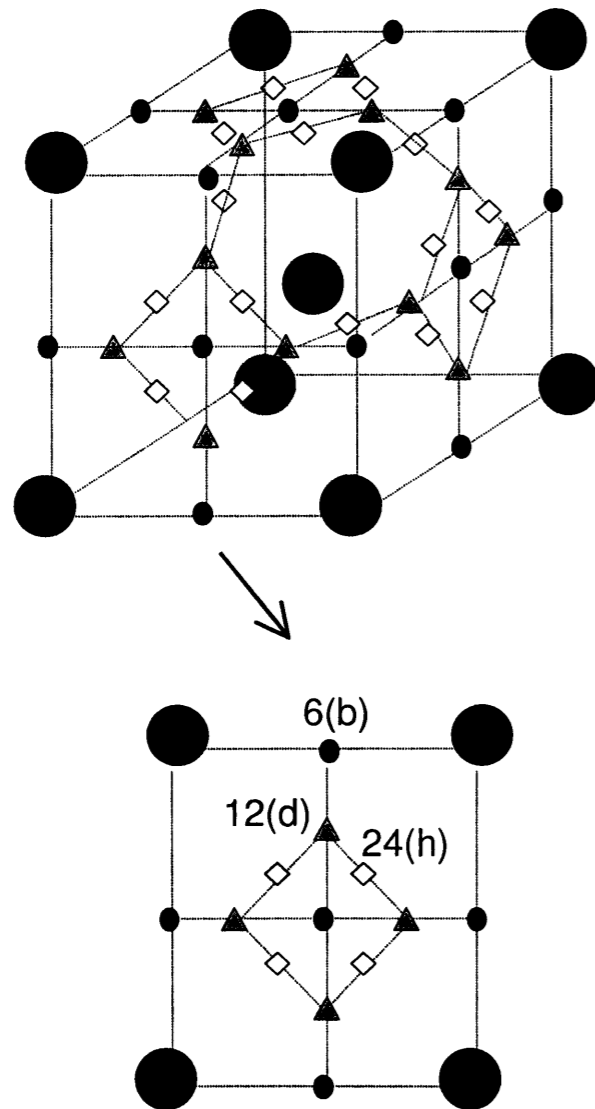
Figure 1.1: The schematic unit lattice in the α-phase. Solid circles ($\bullet$) denote the positions of the iodine ions. $\triangle$, $\Diamond$ and $\bigcirc$ denote the 12(d), 24(h) and 6(b) sites for the cation, respectively.

ionics and it has proved to be a rich source of information. This is not surprising since one of the essential questions is "How do the ion move?" and microscopic techniques like NMR can contribute to the experimental answering this question.

Basic issues in the relationship between NMR and SIC have been discussed and reviewed e.g. by Richards [16] and Boyce and Huberman [17]. These authors described about a general correlation function involving correlation among both distinguishable particles and lattice sites. For a solid AgI crystal, measurement of the ^{109}Ag NMR chemical shift were reported in the temperature range from 180 to 670K by Becker and Goldmmer [18]. The shielding constant of ^{109}Ag was rationalized using a simple tight binding description of chemical bonding. It was concluded that the decreasing paramagnetism of the silver chemical shift was consistent with a distorted tetrahedral coordination of the cations in α-AgI. Endo and co-workers [19–21] also reported experimental and theoretical studies on the chemical shifts of metal NMR for Ag, Cd, Cu and Zn complexes by means of ab initio MO calculation. In the studies, it was indicated the relation between the metal chemical shift and the coordination number in solution and in solid. Thus wealth informations of local structure are obtained from an analysis of the NMR chemical shift.

The direct property of the diffusive motion is obtained from the relaxation study. The relaxation provides motional correlation times, τ, which can be related to microscopic process. The crucial point, however, is to choose an adequate correlation function of the fluctuating local fields, which in turn reflects the ionic dynamics. In other words, the microscopic motion must be modeled. In this point of view, we consider that the MD method can be applied to the NMR spectral analysis. Fukumoto and co-workers discussed about the radial distribution functions and the velocity autocorrelation function in α-AgI by using the MD simulation [12]. It can be expected

that such functions provide us the relation between the NMR spectra and the local structure of the crystal.

The present work is organized as follows. Chapter 2 describes briefly the chemical shift calculation that is based on a finite perturbation method with using the ab initio MO. The ^{109}Ag and ^{63}Cu NMR chemical shifts of $Ag_XCu_{1-X}I$ (X=0, 0.25, 0.5, 0.75, 1.0) crystals are explained as a dependence of the bond length between the metal and iodine by using the finite perturbation method. This work in detail was reported in our recent papers [22-24]. Chapter 3 introduces new idea, "*Average Shielding Value*", into the chemical shift calculation. The assumption is that the chemical shift are estimated by the sum of convolutions of a probability density and a shielding surface, that are based on the neutron diffraction analysis and the ab initio MO calculation, respectively. In chapter 4, the probability density of the cation is calculated by the MD method. From the analysis of the probability density, it is indicated that the chemical shift of the cation is mainly influenced by change of the density at 24(h) sites. The temperature dependences of the chemical shift in α-AgI and α-Ag$_{0.99}$Cu$_{0.01}$I are determined by rapid motion of the cation in the bcc sublattice. Chapter 5 observes the ^{63}Cu NMR spin-lattice relaxation time of α-Ag$_{0.99}$Cu$_{0.01}$I crystal, and simulates the relaxation time from using a distribution of a correlation time of the fluctuating local fields by the MD method. We will also discuss the dynamical structure due to the diffusive motion of the cation in the α-phase.

Chapter 2

Chemical shift calculation for γ-Ag$_X$Cu$_{1-X}$I

The Ag chemical shielding of the silver complex in solution is in considerably good accordance with that in a solid, as obtained in organic compounds that the nuclear chemical shieldings in solution correspond well to the shieldings in a solid. We, accordingly, expect that the experimental metal NMR chemical shieldings of solid metal iodides can be analyzed by using the calculated metal chemical shielding of an isolated metal iodide MI_4^{3-} (M = Ag, Cu) ions in ab initio MO programs.

In the first place, a theoretical derivation of the chemical shielding constant is shown by the finite perturbation method using the ab initio MO. We will use the finite perturbation method throughout this paper. The ^{109}Ag and ^{63}Cu NMR chemical shifts of $Ag_XCu_{1-X}I$ (X=0, 0.25, 0.5, 0.75, 1.0) crystals are explained as a dependence of the bond length between the metal and iodine by the ab initio MO calculation. In the end of this chapter, the electronic structures of the mixed crystal, $Ag_XCu_{1-X}I$, will also be discussed.

2.1 Theoretical Background

The quantum mechanical expression for shielding constant can be derived from finite perturbation theory. The classical energy of interaction between a magnetic moment $\boldsymbol{\mu}$ and a magnetic field $\mathbf{H}$ is given by

$$E = -\boldsymbol{\mu} \cdot \mathbf{H} . \tag{2.1}$$

From this relation and the expression

$$\mathbf{H}_{\text{eff}} = \mathbf{H}_0(1 - \sigma) \tag{2.2}$$

for the effective magnetic field, it can be shown that the shielding constant can be expressed as the appropriate second derivatives of the second-order energy:

$$\sigma_{\alpha\beta} = \frac{\partial^2 E^2}{\partial \mu_\alpha \partial \mathbf{H}_\beta} . \tag{2.3}$$

The total energy of the system is described by the many electron Hamiltonian, Eq.(2.4), which is the modified operator of the kth electron in the presence of a magnetic field. Atomic units ($\hbar = m_e = e = 1$) are used throughout this section.

$$\mathcal{H} = \frac{1}{2} \sum_k^{\text{el.}} \left[-i\nabla_k + \frac{1}{c}\mathbf{A}_k(\mathbf{r}) \right]^2 + V(\mathbf{r}) . \tag{2.4}$$

$$\mathbf{A}_k(\mathbf{r}) = \frac{1}{2}\mathbf{H} \times (\mathbf{r}_{kN} - \mathbf{r}_0) + \left(\frac{\boldsymbol{\mu}_N}{r_{kN}^3} \right) \times \mathbf{r}_{kN} . \tag{2.5}$$

$\mathbf{A}_k(\mathbf{r})$ is the vector potential associated with the kth electron; $\boldsymbol{\mu}_N$ and $\mathbf{H}$ are the nuclear moment and the magnetic field, respectively; $\mathbf{r}_{kN}$ is the distance from the kth electron to the nucleus, while $\mathbf{r}_0$ is the distance from the nucleus to the origin of the vector potential. This origin can be chosen arbitrarily without affecting the exact eigenstates of Eq.(2.4). However, when approximations are introduced in estimating these energies, it is found that in general the choice of origin or gauge is critical to the final results.

Using the standard Rayleigh-Schrödinger procedures, one considers the effects of $\mathbf{H}$ and $\boldsymbol{\mu}$ as small perturbations upon the total energy. The Hamiltonian, wave function ψ, and energy are all expanded in a series of multiorder terms in $\boldsymbol{\mu}$ and $\mathbf{H}$. For the magnetic shielding one requires the second-order energy term which is linear in both $\boldsymbol{\mu}$ and $\mathbf{H}$, as follows

$$E^2(\boldsymbol{\mu}, \mathbf{H}) = \langle \psi^0 | \mathcal{H}^2(\boldsymbol{\mu}, \mathbf{H}) | \psi^0 \rangle + \langle \psi^0 | \mathcal{H}^1(\boldsymbol{\mu}) | \psi^1(\mathbf{H}) \rangle + \langle \psi^0 | \mathcal{H}^1(\mathbf{H}) | \psi^1(\boldsymbol{\mu}) \rangle . \tag{2.6}$$

If the first-order wave function $\psi^1(\mu, \text{or } \mathbf{H})$ is expanded in terms of the excited states of the unperturbed system, the expressions obtained for the diagonal components of σ, using Eq.(2.3), is the Ramsey [25] formula derived for closed-shell states, with similar expressions for the yy and zz components.

$$\sigma_{xx} = \frac{1}{2c^2} \langle \psi^0 | \sum_k \left(\frac{y_{kN}y_k + z_{kN}z_k}{r_{kN}^3} \right) | \psi^0 \rangle$$
$$- \frac{1}{c^2}\mathbf{Re} \sum_{r=1}^{\infty} (E_r - E_0)^{-1} \langle \psi^0 | \sum \frac{M_{xkN}}{r_{kN}^3} | \psi^r \rangle \langle \psi^r | \sum M_{xk} | \psi^0 \rangle \tag{2.7}$$
$$= \sigma_{xx}^{dia} + \sigma_{xx}^{para} . \tag{2.8}$$

M_x is the angular momentum about the x axis; the subscript N indicates that the operator is referred to the resonant nucleus as origin. The sums are over the electron, k, and the excited states, r. $\mathbf{Re}$ specifies the real part. The two terms contained in the expressions for σ are referred to as the diamagnetic and paramagnetic parts. The former depends only upon the ground state wave function and is relatively easy to evaluate. However the paramagnetic terms depend on an infinite sum of excited states including the continuum. In general, to evaluate this term one must rely on some rather uncertain assumptions concerning the availability and accuracy of the excited state wave functions and contributions from higher energy states and the continuum [26]. The most successful theoretical approach in this evaluation is the perturbed Roothaan-Hartree-Fock [27,28] theory for which a very brief outline will be presented.

The form of the theory outlined here will be that for a closed shell molecule, i.e. one with no net electronic angular momentum. The perturbations considered will be the ones involved in the expressions for shielding constant.

It is assumed that a solution to the unperturbed (zero-order) system can be obtained by minimizing the energy defined by

$$E = \langle \psi_{HF} | \mathcal{H} | \psi_{HF} \rangle \,. \tag{2.9}$$

The total Hamiltonian consists of one- and two- electron operators:

$$\mathcal{H} = \sum_{\mu=1}^{2n} h_\mu + \sum_{\mu<\nu}^{2n} \frac{1}{r_{\mu\nu}} \,. \tag{2.10}$$

The Roothaan-Hartree-Fock wavefunction ψ_{HF} is a determinant whose elements ϕ_i are one-electron LCAO-MO's:

$$\phi_i = \sum_{\nu=1}^{p} a_{\nu i} \chi_\nu, \qquad i = 1, 2, \ldots, p \,. \tag{2.11}$$

The linear coefficients of the ϕ_i's are determined from the solution of the set of coupled one-electron Fock equations.

$$F\phi_i = \varepsilon \phi_i, \qquad i = 1, 2, \ldots, p \,. \tag{2.12}$$

where

$$F(\mu) = H(\mu) + G(\mu) \,.$$

The Fock operator $F(\mu)$ is divided into one- and two- electron terms, $H(\mu)$ and $G(\mu)$, respectively, as follows,

$$F(\mu) = \frac{1}{2}\nabla_\mu^2 - \sum_{N}^{\text{nuc.}} \frac{Z_N}{r_{\mu N}} + 2\sum_{j}(2J_j - K_j) \,. \tag{2.13}$$

The coupling between the equations is contained in the Coulomb and exchange operators, J_j and K_j, respectively.

The procedure is used a self-consistent solution of the matrix Roothaan-Hartree-Fock equation.

$$\mathbf{F\,C} = \mathbf{S\,C\,E} \,. \tag{2.14}$$

The total energy of the system, E_{HF}, is expressed as a sum of orbital energies and two-electron integrals over the n occupied MO's,

$$E_{HF} = 2\sum_{i=1}^{n} \varepsilon_i^0 - \sum_{i,j=1}^{n} (2\langle ii|jj \rangle - \langle ij|ij \rangle) \,, \tag{2.15}$$

$$\langle ij|kl \rangle = \int \phi_i(1)\phi_j(1)\frac{1}{r_{12}}\phi_k(2)\phi_l(2)d\tau_1 d\tau_2 \,. \tag{2.16}$$

The quantities $F(\mu)$, ϕ_i and ε_i of Eq.(2.12) are expanded to give a series of perturbation equations. The zero-order equation is assumed to be completely determined the solution. The first-order equation is

$$(F^1 - \varepsilon_i^1)\phi_i^0 = -(F^0 - \varepsilon_i^0)\phi_i^1, \qquad i = 1, 2, \ldots, n \,. \tag{2.17}$$

The perturbed MO's are expanded in terms of the unperturbed virtual (excited) MO's and not the original AO's.

$$\phi_i^1 = \sum_{p=1}^{m} C_{pi}^1 \phi_p^0, \qquad i = 1, 2, \ldots, n \,. \tag{2.18}$$

The first-order coefficients, C_{pi}^1, can be determined by evaluating the matrix elements of F^1 over the zero-order molecular orbital basis and solving the resulting $n \times m$ simultaneous linear equations which, in the presence of the magnetic perturbation operators, have the following form:

$$(\varepsilon_p^0 - \varepsilon_i^0)\mathbf{C}_{pi}^1 + \mathbf{M}_{pi} + \sum_{j=1}^{n}\sum_{q=1}^{m}(\langle qi|pj \rangle - \langle ij|qp \rangle)\mathbf{C}_{qj}^1 = 0, \tag{2.19}$$

$$i = 1, 2, \ldots, n, \quad q = 1, 2, \ldots, m.$$

It can be shown that the second-order energy [28], which determines σ, depends only on the first-order correction to the wave function. The expression for the components of σ is :

$$\sigma_{\alpha\beta} = \frac{1}{c^2}\sum_i \langle \phi_i | \frac{\mathbf{r}_N \mathbf{r}\delta_{\alpha\beta} - r_{N\alpha}r_\beta}{r_N^3} | \phi_i \rangle - \frac{2}{c^2}\sum_i \sum_p (C_{pi}^1)_\alpha \langle \phi_p | \frac{M_{\beta N}}{r_N^3} | \phi_i \rangle \,. \qquad (2.20)$$

The development of the theory followed here is that of Lipscomb, Stevens and Pitzer [28, 29]. An alternate but equivalent derivation of the perturbed Hartree-Fock equations has been given by Pople and co-workers [30,31] who obtained their final working expressions in terms of atomic orbital integrals and zero- and first-order density matrices defined by follows,

$$P_{\nu\lambda}^0 = 2\sum_j^{\text{occ.}} a_{\nu j}^0 a_{\lambda j}^0 \,, \qquad (2.21)$$

$$P_{\nu\lambda}^1 = 2\sum_j^{\text{occ.}} (a_{\nu j}^0 a_{\lambda j}^1 - a_{\nu j}^1 a_{\lambda j}^0) \,. \qquad (2.22)$$

In their scheme the effect of the perturbations upon the molecular orbitals is described in terms of changes in the atomic orbital coefficients. Their final expression for σ corresponding to Eq.(2.20) is :

$$\begin{aligned}\sigma_{\alpha\beta} &= \frac{1}{2c^2}\sum_\nu\sum_\lambda \Big[P_{\nu\lambda}^0 \langle \chi_\nu | \frac{\mathbf{r}_N\mathbf{r}\delta_{\alpha\beta} - r_\alpha r_\beta}{r_N^3} | \chi_\lambda \rangle - 2(P_{\nu\lambda}^1)_\alpha \langle \chi_\nu | \frac{M_{\beta N}}{r_N^3} | \chi_\lambda \rangle \Big] \\ &= \sigma_{\alpha\beta}^{dia} + \sigma_{\alpha\beta}^{para} \,.\end{aligned} \qquad (2.23)$$

From the above and Eq.(2.18), the following are derived an equation for ϕ_j^1, by the Pople and Lipscomb methods.

$$\phi_j^1 = \sum_{p=1}^m C_{pj}^1 \phi_p^0 = \sum_p \sum_\nu C_{pj}^1 a_{\nu p}^0 \chi_\nu \,. \qquad (2.24)$$

The finite perturbation method is able to give good results using very large basis sets and reasonable results for many small molecules using moderate-sized basis sets. One of the deficiencies of this approach was that the molecular and atomic orbital integrals

and hence the shielding depended on the origin of the magnetic vector potential. It is possible to eliminate the gauge dependence of the computed shielding tensor by using atomic orbitals containing explicit vector potential factors [32]:

$$\begin{aligned}\xi_\nu(\mathbf{H},\mathbf{r}) &= \exp\Big[-\frac{i}{c}\mathbf{A}_\nu(\mathbf{r})\cdot\mathbf{r}\Big]\chi_\nu(\mathbf{r}) \,, \qquad (2.25)\\ \mathbf{A}_\nu(\mathbf{r}) &= \frac{1}{2}\mathbf{H}\times\mathbf{r}_\nu \\ &= \frac{1}{2}\mathbf{H}\times(\mathbf{r} - \mathbf{R}_\nu) \qquad (2.26)\end{aligned}$$

where $\mathbf{R}_\nu$ is the distance from the arbitrary origin to the atom on which the AO is centered. This approach, first used by London [33], is known as the gauge-invariant atomic orbitals method (GIAO).

Ditchfield has recently developed a theory which utilizes GIAO within the perturbed Hartree-Fock framework [34, 35]. Since the atomic orbitals contain a field dependence, and the overlap, core, and two-electron integrals, as well as the expansion coefficients and the density matrix, will depend explicitly on the magnetic field. The total energy of the system in the presence of the perturbations μ_N and $\mathbf{H}$ (using Pople's formalism) is

$$E(\mathbf{H},\mu_N) = \sum_{\mu,\nu} P_{\mu\nu}H_{\mu\nu}^{\text{core}} + \frac{1}{2}\sum_{\mu,\nu}P_{\mu\nu}G_{\mu\nu} \,. \qquad (2.27)$$

Recalling the definition of σ as second derivatives of the energy, one sees that the use of gauge-dependent AO's will yield several additional terms to their expressions. The expression corresponding to Eq.(2.23) for the magnetic shielding is [30]

$$\begin{aligned}\sigma_{\alpha\beta} &= \frac{1}{2c^2}\sum_\nu\sum_\lambda \Big[P_{\nu\lambda}^0 \langle \chi_\nu | \mathbf{r}_\mathbf{N}\cdot(\mathbf{r}-\mathbf{R}_\nu)\delta_{\alpha\beta} - r_{N\alpha}(r-R_\nu)_\beta | \chi_\lambda \rangle \\ &\quad + P_{\nu\lambda}^0 \langle \frac{\partial\xi_\nu}{\partial H_\alpha} | \frac{M_{\beta N}}{r_N^3} | \chi_\lambda \rangle + P_{\nu\lambda}^0 \langle \chi_\nu | \frac{M_{\alpha N}}{r_N^3} | \frac{\partial\xi_\lambda}{\partial H_\beta} \rangle \\ &\quad + (P_{\nu\lambda}^1)_\alpha \langle \chi_\nu | \frac{M_{\beta N}}{r_N^3} | \chi_\lambda \rangle \Big] \,. \qquad (2.28)\end{aligned}$$

since one requires only a single derivative with respect to $\mathbf{H}$ for the first order density matrix, $(P^1_{\nu\lambda})_\alpha$, it is sufficient to retain terms only up to linear powers of $\mathbf{H}$ in the evaluation of the requires integrals. A general integral of the form $\langle\mu|\hat{O}|\nu\rangle$ is expanded as follows [34]:

$$\int \xi^*_\mu \hat{O} \xi_\nu d\tau = \int \exp\left[\frac{i}{c}(\mathbf{A}_\mu - \mathbf{A}_\nu)\cdot\mathbf{r}\right]\chi_\mu\hat{O}\chi_\nu d\tau$$
$$= \int \chi_\mu\hat{O}\chi_\nu d\tau - \frac{1}{2c}\mathbf{H}\times(\mathbf{R}_\mu - \mathbf{R}_\nu)\cdot\int\mathbf{r}\chi_\mu\hat{O}\chi_\nu d\tau . \qquad (2.29)$$

Thus the integrals to be evaluated contain an additional factor of $\mathbf{r}$ in the integrand.

The results using GIAO theory have been extremely good. Ditchfield has shown that even using a minimal Gaussian-type orbital (GTO) basis set of GIAO one obtains results which are in better overall agreement with the experimental values than the moderately extended sets [35].

2.2   Experimental in γ-phase

Ida and co-workers [23] measured the ^{109}Ag MAS NMR spectra at a frequency of 12.45 MHz, using a JEOL GX-270 spectrometer. 120 transients were accumulated using an 8.5 μs (90°) pulse. The spectra were obtained under magic-angle spinning at a speed of about 5 kHz; 8 k data points were collected over bandwidths of 20 kHz. All measurements were carried out at 300 K and solid AgI was used as an external reference.

Crystalline Ag$_x$Cu$_{1-x}$I in which the solid solution was complete was prepared by a melt annealing method in a vacuum vessel to prevent oxidation. The Ag/Cu for mixed crystals was estimated using an X-ray fluorescence method.
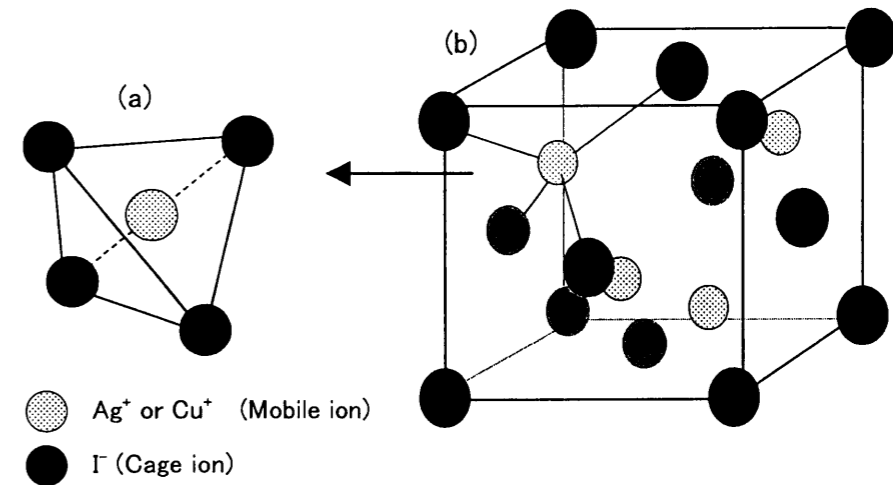
Figure 2.1: (a) The isolated complex ion model and (b) the schematic crystal structure of γ-Ag$_x$Cu$_{1-x}$I

2.3   Computational

As the structural data of tetrahedral AgI$_4^{3-}$ and CuI$_4^{3-}$ complex ions in the γ-phase, we used the lattice constants of Ag$_x$Cu$_{1-x}$I crystals determined by X-ray diffraction measurements [36]. The coordinations in MI$_4^{3-}$ (M = Ag, or Cu) ions were estimated as M(0, 0, 0), I($-c/4$, $-c/4$, $-c/4$), I($-c/4$, $c/4$, $c/4$), I($c/4$, $-c/4$, $c/4$) and I($c/4$, $c/4$, $-c/4$), where c denotes the lattice constant in the γ-phase. The unit lattice constants (c) was used as (6.20, 6.30, 6.39, and 6.48 Å) for a T$_d$ AgI$_4^{3-}$ complex ion, and (6.08, 6.20, 6.30, and 6.39 Å) for a T$_d$ CuI$_4^{3-}$ ion, respectively. The isolated complex ion model and the schematic crystal structure of γ-Ag$_x$Cu$_{1-x}$I is shown in Fig.2.1. Ag and Cu chemical shielding constants were calculated by the finite-perturbation method using the Gaussian 94 program [37] together with a DZVP basis set [38] for the Ag, Cu, and I atoms. Then, ab initio MO calculations were performed on a DEC VT-Alpha 533 workstation.

2.4 Results and Discussion for Ag$_x$Cu$_{1-x}$I

Complete solid solution Ag$_x$Cu$_{1-x}$I crystals in a zincblende structure was obtained, as indicated by the X-ray diffraction measurement [36]. The ^{109}Ag and ^{63}Cu MAS NMR signals of the Ag$_x$Cu$_{1-x}$I crystals shown in Fig.2.2 (a) and (b), respectively, and Table 2.1 summarized the shift values with broadening to a low field relative to AgI and Ag$_{0.75}$Cu$_{0.25}$I. It is emphasized that the low-field shifts of the Ag and Cu signals were observed linearly with decreasing the lattice constant of the mixed crystals shown in Table 2.1. Endo and co-workers reported experimental and theoretical studies on the chemical shifts of metal NMR for metal complexes in solution and solid [19-21]. Accordingly we consider that the metal low field shift with decreasing the lattice constant will be explained by the ab initio MO calculations of isolated MI$_4^{3-}$ (M = Ag, Cu) complex ions. The bond length, $R_{Ag,Cu-I}$, in MI$_4^{3-}$ (M = Ag, Cu) was calculated from the unit lattice constants of Ag$_x$Cu$_{1-x}$I (x = 0.0, 0.25, 0.50, 0.75, 1.0) given in Table 2.1.

The Ag and Cu nuclear shielding constants and chemical shifts in MI$_4^{3-}$ (M = Ag, Cu) with the observed chemical shifts in Ag$_x$Cu$_{1-x}$I crystals (x = 0.0, 0.25, 0.50, 0.75, 1.0) were summarized in Table 2.2. The calculated Ag and Cu shifts are given relative to the reference molecules, AgI$_4^{3-}$ (R_{Ag-I} = 2.81 Å) and CuI$_4^{3-}$ (R_{Cu-I} = 2.77 Å), respectively. In the table, it is given the observed Ag and Cu shifts of Ag$_x$Cu$_{1-x}$I relative to the AgI and Ag$_{0.75}$Cu$_{0.25}$I, respectively. The calculated Ag and Cu chemical shieldings in MI$_4^{3-}$ (M = Ag, Cu) are dominated by the paramagnetic term, since the diamagnetic terms are constant (σ_{dia} = 4679 - 4680, and 2406 ppm for AgI$_4^{3-}$ and CuI$_4^{3-}$, respectively). For both metal complexes, the calculated shifts reflect the observed qualitative trends well to the low field.
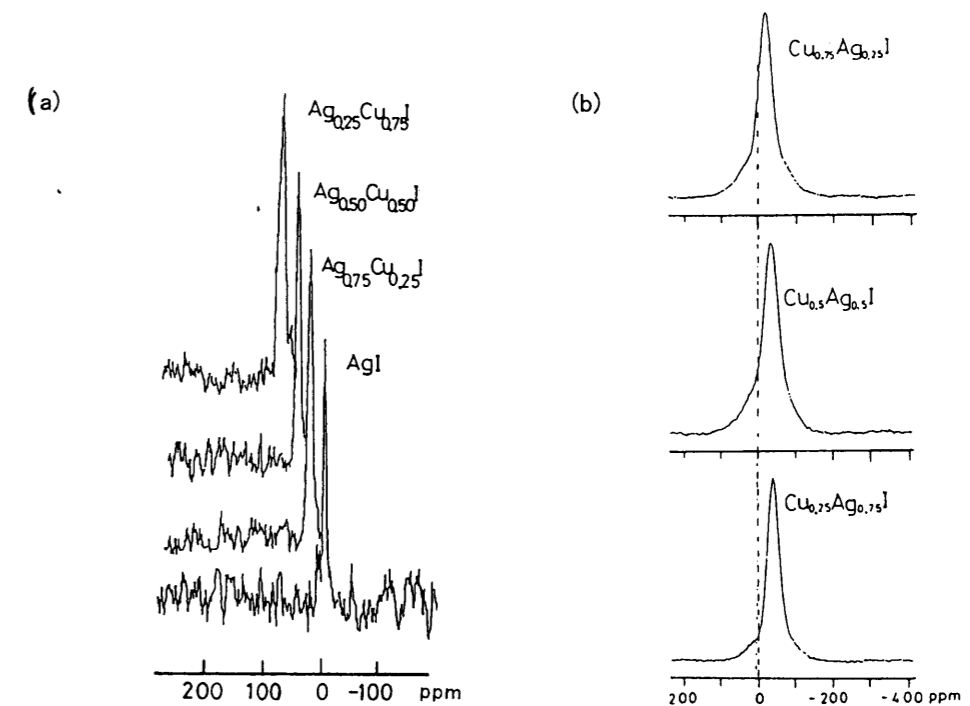
Figure 2.2: (a) ^{109}Ag and (b) ^{63}Cu MAS NMR spectra of Ag$_x$Cu$_{1-x}$I crystal at room temperature.

Table 2.1: Observed Ag and Cu chemical shifts, half-line widths, and unit lattice constants of Ag$_x$Cu$_{1-x}$I crystal.

		Ag$_x$Cu$_{1-x}$I crystal			
	CuI	Ag$_{0.25}$Cu$_{0.75}$I	Ag$_{0.5}$Cu$_{0.5}$I	Ag$_{0.75}$Cu$_{0.25}$I	AgI
Ag Chemical Shift (ppm)		72.6	43.1	28.0	0.0
Ag half-linewidth (Hz)		200	120	120	85
Cu Chemical Shift (ppm)	32.9	18.8	6.0	0.0	
Cu half-linewidth (Hz)	256	1608	1805	1427	
unit lattice constant (Å)	6.08	6.20	6.30	6.39	6.48

2.4.1 Bond length dependence of chemical shift

Let's consider the reason why the calculated values of the isolated complex ions are not in quantitative agreement with the observed ones. The calculated shieldings of isolated MI_4^{3-} seem to be overestimated in comparison with the observed shifts in solid $Ag_xCu_{1-x}I$, because the electron donations from iodines to metal ions, and back donations to iodines from d-electron of metal ions due to repetitive ion structures in solid, become considerably less than those in the isolated complex ions. It is expected that the results reflect the paramagnetic terms dominantly. A more quantitative accordance may be obtained at least by reflecting a lattice vibration of the metal on the calculation, or by performing ab initio MO calculations of the MI_4^{3-} ion including the nearest-neighbor MI_4^{3-} complex ions.

2.4.2 Electronic states

In order to clarify the theoretical reason for the low field shifts and the roles of the electrons in the chemical bonds of Ag- and Cu-iodide complexes, we examined the change in the valence atomic orbital (AO) densities of the Ag and Cu ions and I in MI_4^{3-} (M = Ag, Cu). The results are given in Table 2.3. In this table, the total density increases in the ns and np AOs of Ag ($n = 5$) and Cu ($n = 4$) atoms and the density decreases in the s and p AOs of iodine atoms indicate electron transfers from the iodines to metal atoms. Back donations to iodines also produce holes in the $(n-1)$d orbitals of Ag ($n = 5$) and Cu ($n = 4$) atoms due to $d\pi$(metal) - $p\pi$(ligand) interaction of metal iodide complexes. It is interesting that the metal chemical shielding constants depend on the electron and hole density increases in the valence s, p and d orbitals of metal atoms with decreasing the bond length between the metal and iodine atoms.

Table 2.2: Calculated Ag and Cu chemical shielding constants and the shifts of T_d AgI_4^{3-} and T_d CuI_4^{3-} complex ions, respectively with observed chemical shifts of $Ag_xCu_{1-x}I$ crystal

MI_4^{3-} complex	calculated shielding constant			shift	$Ag_xCu_{1-x}I$	observed shifts
R_{M-I}	σ_{dia}	σ_{para}	σ_{total}			
(Å)	(ppm)	(ppm)	(ppm)	(ppm)		(ppm)
Ag shielding constant						
AgI_4^{3-} (2.81)	4679	-1272	3407	0	AgI	0.0
AgI_4^{3-} (2.77)	4679	-1370	3309	98	$Ag_{0.75}Cu_{0.25}I$	28.0
AgI_4^{3-} (2.73)	4680	-1472	3208	199	$Ag_{0.50}Cu_{0.50}I$	43.1
AgI_4^{3-} (2.68)	4680	-1588	3092	315	$Ag_{0.25}Cu_{0.75}I$	72.6
Cu shielding constant						
CuI_4^{3-} (2.77)	2406	-695	1711	0	$Ag_{0.75}Cu_{0.25}I$	0.0
CuI_4^{3-} (2.73)	2406	-744	1662	49	$Ag_{0.50}Cu_{0.50}I$	6.0
CuI_4^{3-} (2.68)	2406	-806	1600	111	$Ag_{0.25}Cu_{0.75}I$	18.8
CuI_4^{3-} (2.63)	2406	-878	1528	183	CuI	32.9

Table 2.3: The change* in total AO densities of T_d AgI$_4^{3-}$ and T_d CuI$_4^{3-}$ complex ions.

orbital	MI$_4^{3-}$	MI$_4^{3-}$	MI$_4^{3-}$	MI$_4^{3-}$	MI$_4^{3-}$
$R_{M-I} =$	2.81Å	2.77Å	2.73Å	2.68Å	2.63Å
AgI$_4^{3-}$ complex					
silver					
4d	-0.0480	-0.0738	-0.1014	-0.1343	
5s	0.0905	0.1022	0.1137	0.1262	
5p	0.2679	0.2824	0.2977	0.3160	
iodine					
5s	-0.0418	-0.0474	-0.0530	-0.0591	
5p	-0.0529	-0.0523	-0.0514	-0.0503	
CuI$_4^{3-}$ complex					
copper					
3d		-0.0672	-0.0854	-0.1098	-0.1406
4s		0.1423	0.1524	0.1654	0.1810
4p		0.2917	0.3132	0.3422	0.3789
iodine					
5s		-0.0268	-0.0331	-0.0411	-0.0508
5p		-0.0760	-0.0781	-0.0807	-0.0841

* The change of the density was evaluated relative to densities of each atomic orbital in the neutral atom.

As reported earlier for solution [109]Ag and [63]Cu NMR studies [20, 21], the chemical shieldings of silver- and copper-iodide complexes can be governed by the paramagnetic term. This will be explained by the following equation for [109]Ag and [63]Cu chemical shieldings:

$$\sigma_{para} = \left(\frac{-2\alpha^2}{3}\right)\left[\left(\frac{\langle 1/r^3\rangle_p\, P_T^e}{E_p}\right) + \left(\frac{\langle 1/r^3\rangle_d\, 3D_T^h}{E_d}\right)\right],\qquad (2.30)$$

where P_T^e and D_T^h are the total populations of the p electrons and d holes, respectively.

The contributions to the paramagnetic term for Ag and Cu shieldings can be estimated from $E_{p,d}$ and $\langle 1/r^3\rangle_{p,d}$ as parameters in Eq.(2.30). We assume that $E_p \simeq E_d$, $\langle 1/r^3\rangle_{np} = 1.38$ or 0.59 a.u. and $\langle 1/r^3\rangle_{(n-1)d} = 3.67$ or 5.00 a.u. for Ag ($n = 5$) or Cu ($n = 4$), respectively. (The terms were obtained from the SCF functions by Clementi and coworkers [39].

Thus, the contributions to the paramagnetic shielding constants of the Cu and Ag for T_d MI$_4^{3-}$ (M = Cu, Ag) complexes was showed in Table 2.4. It follows from this table that for Ag complexes the p and d contributions are relatively close and competitive, and for the Cu complexes the d contributions are larger than the p contributions.

Table 2.4: Contributions to the paramagnetic term of the Ag and Cu shielding constants from the valence d and p AO for T_d MI_4^{3-} complex ions.

orbital	MI_4^{3-}	MI_4^{3-}	MI_4^{3-}	MI_4^{3-}	MI_4^{3-}
R_{M-I} =	2.81Å	2.77Å	2.73Å	2.68Å	2.63Å
AgI_4^{3-} complex					
4d-contribution					
($2\alpha^2/3E_d$) unit	-0.530	-0.811	-1.118	-1.479	
5p-contribution					
($2\alpha^2/3E_p$) unit	-0.370	-0.390	-0.411	-0.436	
CuI_4^{3-} complex					
3d-contribution					
($2\alpha^2/3E_d$) unit		-1.007	-1.281	-1.647	-2.111
4p-contribution					
($2\alpha^2/3E_p$) unit		-0.172	-0.185	-0.202	-0.224

Chapter 3

Analysis of temperature dependence of chemical shift

In previous chapter, the calculation technique of the chemical shift was shown for the finite perturbation theory using the ab initio MO program. In the calculation of the chemical shift, we assumed the isolated complex ion, MI_4^{3-} (M = Ag or Cu), as a model of the $Ag_xCu_{1-x}I$ crystal. It was concluded that the chemical shifts came from a change in the bond length between the metal and iodine.

Recently, the shielding values obtained from ab initio calculations [40–42] have been getting quantitatively closer to the experimental ones for a molecule within a fraction of a ppm. Shielding calculation is usually done for an isolated molecule in equilibrium geometry. However if this procedure was applied to solid-state compounds, the most calculated results reproduced only the observed trends of the chemical shift, or disagreed with the experimental ones. For a solid state, the shielding values are influenced by a deriving effect resulting from a point defect, a thermal vibration and a diffusion, and these effects are strongly depended on a temperature. Therefore, it is

necessary to consider a new calculation method for solids.

3.1 Average shielding value calculation

The lattice constants of AgI crystal were little change over the γ-phase from X-ray structure analysis by Kimura [36], as shown in Fig.3.1. The lattice constant in γ-phase was about 6.48Å. That of α-AgI crystal also unchanged with increasing temperature; it was 5.07Å. Whereas Becky and co-worker reported that the solid-state ^{109}Ag NMR signals of AgI shifted to high field with increasing temperature and obtained the similar slopes of 0.33 ppm/K in both phases [18]. Namely the bond length between the silver and iodine atoms was no change; nevertheless the chemical shielding values of the Ag atom indicated the high field shift with increasing temperature. The purpose of this chapter is in particular to examine the origin for the temperature dependence of the Ag chemical shift in AgI crystal by introducing a concept of an "*Average shielding value*".

We considered that the "*density of atom*" at temperature T can be written as $\rho(\mathbf{R}, T)$, where $\mathbf{R}$ is the nuclear positions and $\rho(\mathbf{R}, T)dv$ is the probability density of atom, then the average shielding value at temperature T, $\sigma^{\mathrm{ave}}(T)$, is

$$\sigma^{\mathrm{ave}}(T) = \int_{\mathrm{unit}} \sigma(\mathbf{R})\rho(\mathbf{R}, T)dv \tag{3.1}$$

where the integration is over the range of one unit lattice in the crystal. The AgI crystal consists of the cage (iodine) and the mobile (silver) ions. If the cage ions are rigid, $\mathbf{R}$ is referred to only the mobile ions position. Thus, the $\rho(\mathbf{R}, T)$ and the $\sigma(\mathbf{R})$ are defined as a "density" and a "shielding surface" of only the mobile ion, respectively, in the rigid sub-lattice of the iodine.

The shielding surface, which is applied to the present calculation, is mathematical description of how the shielding (or chemical shift) property changes with the internal
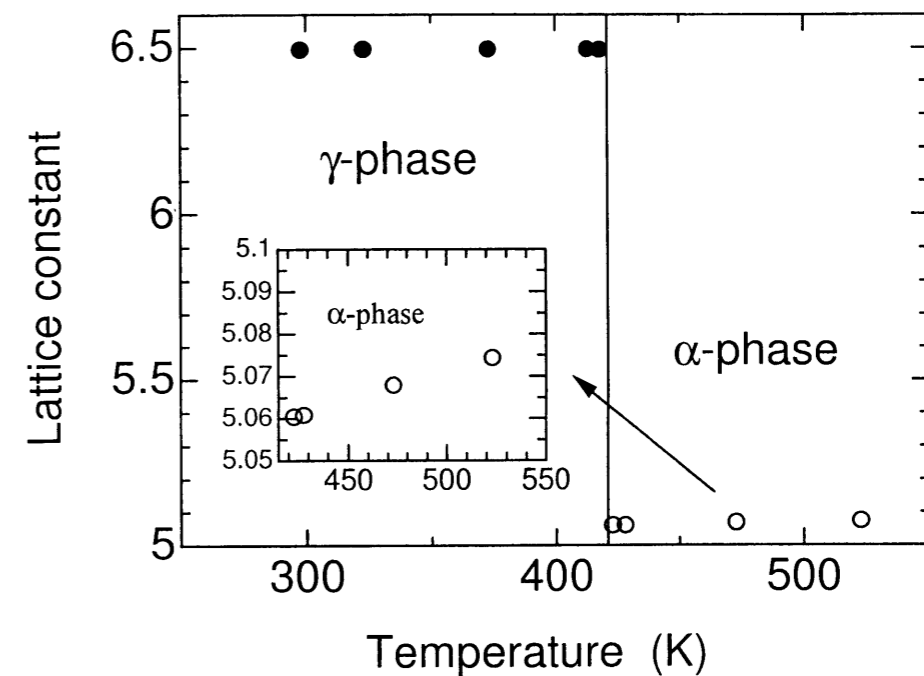

Figure 3.1: Temperature dependence of the lattice constant for AgI crystal in ref. [36].

coordinates of atoms in a molecule, cluster of molecules, or a crystal. For intramolecular effects, the shielding may be expressed as a function of bond lengths, bond or torsion angles, and displacements from equilibrium position. The simplest shielding surface, and identically the first one to be calculated was for the H_2^+ molecule [43]. In recent paper [44], Le and co-workers determined a protein secondary structure by creating a map of how the shielding changes with two torsion angles in a fragment such as N-formyl alanine amido. The map was called "*Ramachandran shielding surface*". Although the shielding surface has been applied to some theoretical NMR works in small or organic molecules, no studies have ever tried to calculate a map of the metal chemical shifts.

3.2 γ-phase

In the γ-phase, if the atoms in the crystal slightly vibrate about their equilibrium positions $\mathbf{R_e}$, with an amplitude which increses with temperature, then the probability density $\rho(\mathbf{r}, T)$ with respect to the displacement $\mathbf{r} = \mathbf{R} - \mathbf{R_e}$ is

$$\rho(\mathbf{r}, T) = N_0^{-1} \exp\left[-\frac{1}{2}\sum_{i=1}^{3}\left(\frac{\mathbf{r}_i}{U_{ii}(T)}\right)^2\right], \tag{3.2}$$

where

$$N_0 = (8\pi^3 U_{11} U_{22} U_{33})_T^{-1}, \tag{3.3}$$

and $\mathbf{U}_{ii}$ is the harmonic temperature factor. For detailed arguments of the probability density function, see Appendix A.

The shielding surface can be expanded in a Taylor series in terms of displacements around the equilibrium position $\mathbf{r} = 0$ as follows:

$$\begin{aligned}
\sigma(\mathbf{r}) &= \sigma(0) + \sum_{i}^{3}\left(\frac{\partial\sigma}{\partial\mathbf{r}_i}\right)_{\mathbf{r}=0}\mathbf{r}_i + \sum_{i,j}^{3}\frac{1}{2}\left(\frac{\partial^2\sigma}{\partial\mathbf{r}_i\partial\mathbf{r}_j}\right)_{\mathbf{r}=0}\mathbf{r}_i\mathbf{r}_j + \cdots \\
&= \sigma^{(0)}(0) + \sum_{i}\sigma^{(1)}(0)\mathbf{r}_i + \sum_{i,j}\sigma^{(2)}(0)\mathbf{r}_i\mathbf{r}_j + \cdots.
\end{aligned} \tag{3.4}$$

Table 3.1: **Temperature dependence of the isotropic temperature factors for γ-AgI. The isotropic factor is defined as $U = \frac{1}{3}(U_{11} + U_{22} + U_{33})$.**

Temp.	U
(K)	(Å²)
300	0.0773
353	0.0963
413	0.124

Refered from [2].

where $\sigma^{(0)}(0)$ is a zero-order shielding value at the equilibrium position. In the previous chapter, it was regarded as the chemical shielding value of Ag or Cu atoms for the γ-$Ag_X Cu_{1-X}I$.

Substituting Eqs.(3.2) and (3.4) into the Eq.(3.1), the average shielding value is given by

$$\begin{aligned}
\sigma^{\text{ave}}(T) &= \int_{\text{unit}} N_0^{-1}\exp\left[-\frac{1}{2}\sum_{i=1}^{3}\left(\frac{\mathbf{r}_i}{U_{ii}(T)}\right)^2\right] \\
&\quad \times \left(\sigma^{(0)}(0) + \sum_{i}\sigma^{(1)}(0)\mathbf{r}_i + \sum_{i,j}\sigma^{(2)}(0)\mathbf{r}_i\mathbf{r}_j + \cdots\right)dv \\
&= \sigma^{(0)}(0) + \sum_{i}\left[U_{ii}(T)\,\sigma^{(2)}(0)\right] + \cdots.
\end{aligned} \tag{3.5}$$

This equation indicates that the temperature dependence of the chemical shielding value is depended on even-order coefficients of the expanded shielding surface and the temperature factor. The temperature factors of γ-AgI were reported in the neutron diffraction study by Cave and co-workers [2], and is listed in Table 3.1. These factors was estimated by using Zachariasen's model [45].

3.2.1   Computational

The shielding surface was also evaluated by the finite perturbation method based on ab initio MO method. Isolated complex ion $[AgI_4]^{3-}$ was employed to the model of γ-AgI crystal. Four I^- ions were arranged at positions of $(c/4, \sqrt{2}c/4, 0)$, $(c/4, -\sqrt{2}c/4, 0)$, $(-c/4, 0, \sqrt{2}c/4)$ and $(-c/4, 0, -\sqrt{2}c/4)$ where c is the lattice constant and the x-y plane is (110) plane of the zincblende type crystal in the γ-phase. Positions $(x, y, 0)$ of Ag^+ ion were varied from -0.5 to 0.5Å in calculating the shielding values and the origin is the equilibrium position. Step size is 0.10Å for each direction. The schematic complex ion model is shown in Fig.3.2. Calculations were performed at Hartree-Fock level. The basis sets used for Ag and I atoms were DZVP [38] and LANL2DZ [46], respectively. The calculations of the chemical shielding value were carried out with Gaussian 98 [47].

3.2.2   Results and discussion for γ-AgI

Fig.3.3 shows a contour plot of the Ag NMR chemical shielding surface on (110) plane of the AgI crystal. The figure indicated that a shielding value at the equilibrium position was the highest; in other words, the shift was the lowest field. The calculated high field shifts were isotropic for small displacement from the equilibrium position. In previous chapter, the high field shift came from the increasing bond length between silver and iodine atoms, in this chapter the high field shifts due to the displacement of the cation from the equilibrium position. In order to examine a displacement dependence of the chemical shift, the calculated shift value vs. the displacement on O-P line in Fig.3.3 were plotted in Fig.3.4. From the figure, best fit parameters in Eq.(3.4) were estimated as $\sigma^{(2)} = -453$ relative to the value at the equilibrium potion. The average
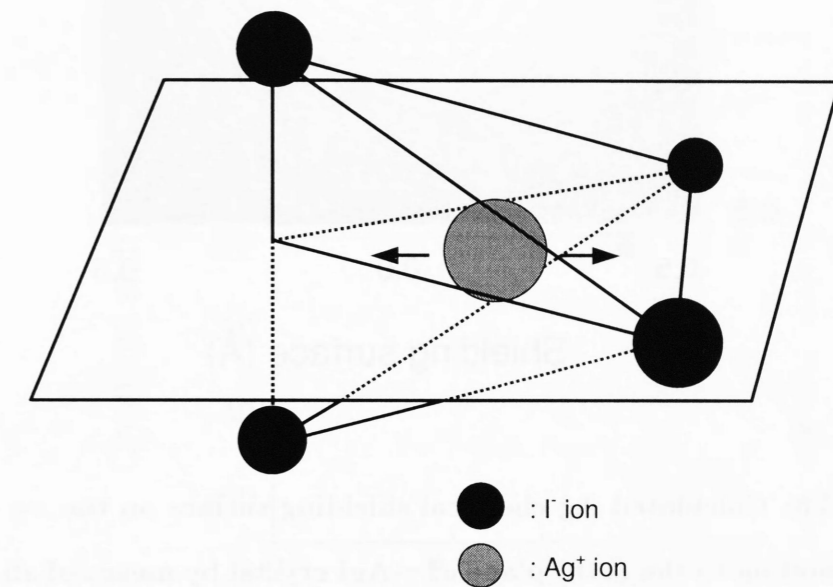
Figure 3.2: The isolated complex ion model for γ-AgI. Four I atoms are located at positions of $(c/4, \sqrt{2}c/4, 0)$, $(c/4, -\sqrt{2}c/4, 0)$, $(-c/4, 0, \sqrt{2}c/4)$ and $(-c/4, 0, -\sqrt{2}c/4)$ where c is the lattice constant (6.48Å). One Ag atom located on the $x - y$ plane.
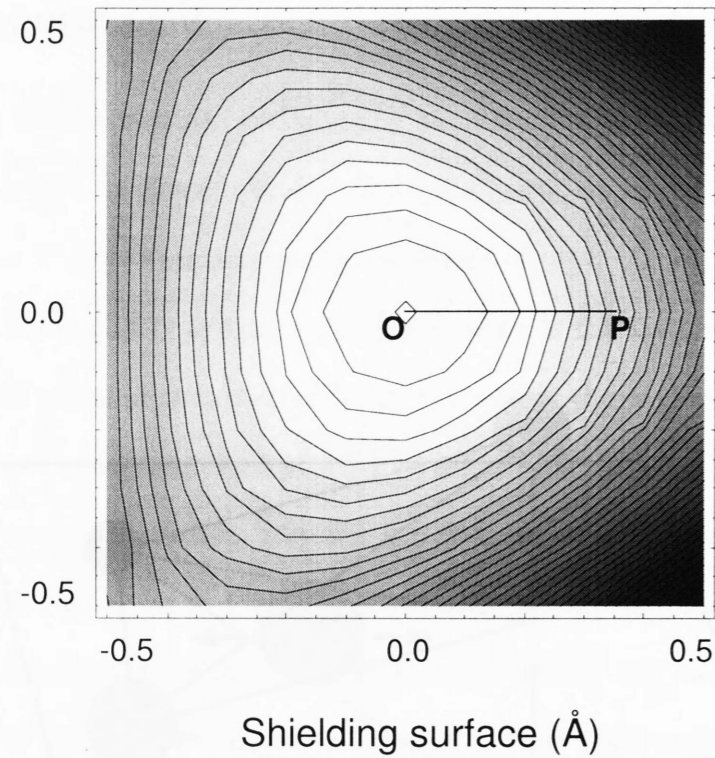
Figure 3.3: Calculated Ag chemical shielding surface on the x-y plane corresponding to the (110) plane of γ-AgI crystal by means of ab initio MO program with basis sets DZVP and LANL2DZ for Ag and I atoms, respectively.

shielding values can be calculated by substituting the temperature factor and the zero- and second-order coefficients $\sigma^{(0,2)}$ into Eq.(3.5). The calculated Ag chemical shifts were given relative to the reference shielding value at 300K. Comparison between the calculated and the observed values of Ag chemical shifts at 353 and 413K are shown in Fig.3.5. From the figure, the calculated shifts reflect the observed qualitative trend well to the high field.

For the present, it is concluded that the observed [109]Ag high field shifts in the γ-AgI crystal are influenced by the spreading density distribution of the cation with increasing
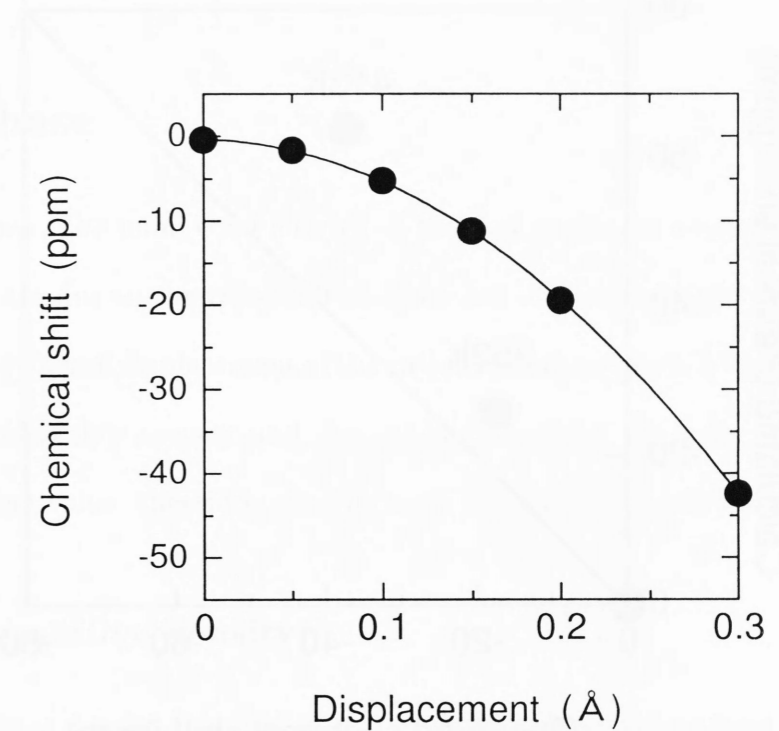

Figure 3.4: Displacement dependence of Ag chemical shift value on O–P line in Fig.3.3. Solid line is optimized by least square method and provides for $\sigma^{(0)} = 0$ and $\sigma^{(2)} = -453$.
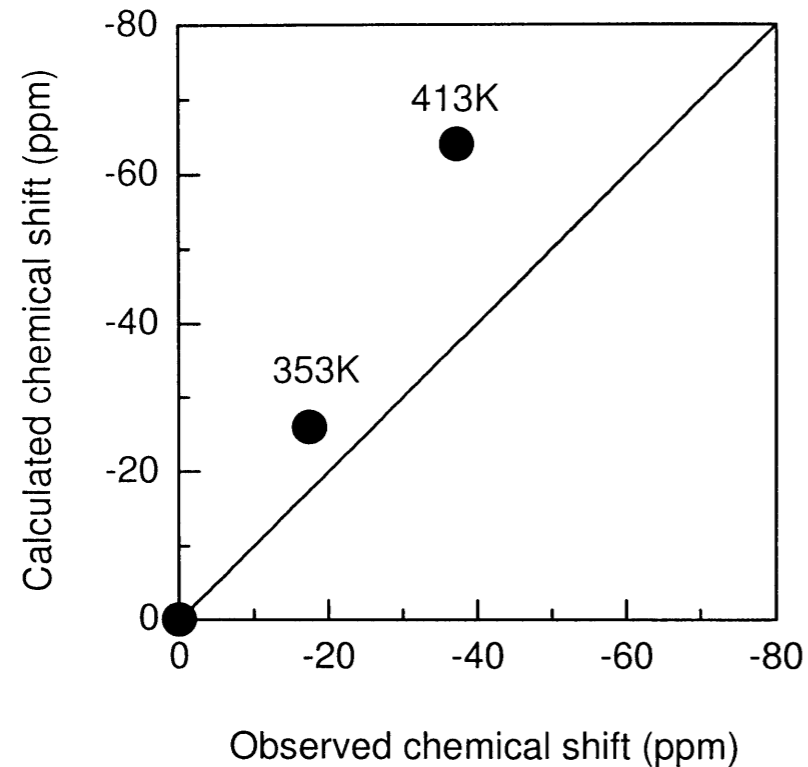
temperature, since the equilibrium structure and crystal symmetry are no change.

Clearly the temperature factor in the γ-phase is mainly due to thermal vibration of atoms. In the α-phase, Ag atoms not only vibrate, but also rapidly diffuse in the AgI crystal. Let us discuss the chemical shifts including an effect of the diffusive motion, in the next section.

3.3 α-phase

In the α-phase, the ionic conductivity of the AgI crystal is comparable to that of liquid electrolytes due to the rapid diffusive motion of silver ions. So the Taylor series expansion for the small displacement of the cation cannot be applied for the calculations of both the probability density and the shielding surface. In order to calculate the average shielding value, therefore, we will begin the numerical calculation of Eq.(3.1).

3.3.1   Probability density

The probability density function in the α-phase is more generalized and evaluated by using the temperature factor which was also reported by Cave and co-workers [2]. The general probability density function $\rho(\mathbf{r})$ is given by

$$\rho(\mathbf{r}) = \rho_0(\mathbf{r})\left[1 + \frac{1}{3!}c^{jkl}H_{jkl}(\mathbf{r}) + \frac{1}{4!}c^{jklm}H_{jklm}(\mathbf{r}) + \ldots\right] \tag{3.6}$$

where $\rho_0(\mathbf{r})$ is Gaussian type function, $c^{j\cdots}$ are the elements of the temperature factor which are summarized in Table 3.2, and $H_{j\ldots}(\mathbf{r})$ are linear combinations of Hermite polynomials, see appendix A. The probability density of the silver ion on the (100) plane of α-AgI crystal was calculated by using the temperature factors and is shown in Figs.3.6. The figure indicated that the density of the silver ion mainly located at

Figure 3.5: **Comparison between the calculated and the observed values of Ag chemical shifts at 353 and 413K. The Ag chemical shifts are given relative to the reference shielding value at 300K.**

Table 3.2: Temperature factors for α-AgI. Ag^+ ions occupy positions 12(d) (1/4,0,1/2) of space group Im3m.*

Temp.	U_{11}	U_{22}	c_{122}**	c_{1111}***
(K)			$(\times 10^3)$	$(\times 10^4)$
473	0.316	0.170	−0.375	1.160
513	0.342	0.192	−0.491	2.400
573	0.367	0.198	−0.423	—

* : Refered from [2]

** : $c_{122} = -c_{133}$; all other $c_{jkl} = 0$.

*** : Other $c_{jklm} = 0$, omitted values were not siginificant.

the 12(d) sites and together with some densities at the 24(h) and the 6(b) positions. Figs.3.6 (a) and (b) show the probability density of Ag atom at 473 and 573K, respectively. It appeared that density distributions of Ag atom were broadened with increasing temperature. The broadening is influenced by the thermal vibration and the diffusion of the mobile ion. The distributions show intricate temperature dependence, therefore we use numerical density set of Ag atom as the probability density. Then, the Eq.(3.1) is deformed to a discrete expression as follows

$$\sigma^{\mathrm{ave}}(T) = \sum_{i,j,k}^{\mathrm{unit}} \sigma(x_i, y_j, z_k) \times \rho(x_i, y_j, z_k, T) . \qquad (3.7)$$

where the shielding surface is similaly deformed to the discrete expression.

3.3.2   Shielding surface

The computation of the shielding surface in the α-phase was carried out with the same methods in the γ-phase, except a model molecule. The model of the α-AgI
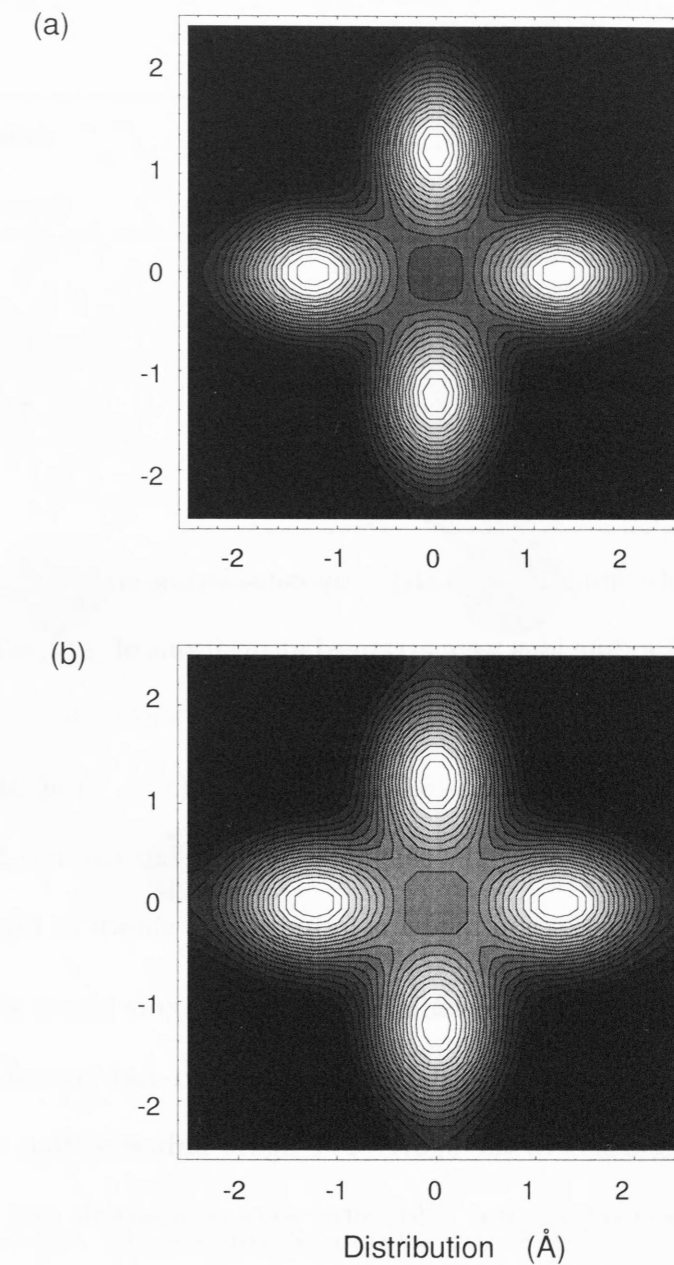

Figure 3.6: Distribution of silver scattering density at (a) 473K and (b) 573K on (001) plane of the α-AgI crystal by the neutron-diffraction study [2].

Table 3.3: Calculated Ag chemical shielding values at the 6(b), 12(d) and 24(h) sites. The chemical shifts are given relative to the shielding value in the 12(d) site.

site	σ_{dia}	σ_{para}	σ_{total}	shift
	(ppm)	(ppm)	(ppm)	(ppm)
6(b)	4679	−1054	3625	9
12(d)	4677	−1061	3616	0
24(h)	4679	−1134	3545	−71

crystal employed isolated complex ion $[AgI_8]^{7-}$ by considering structure symmetry of fixed iodine atoms. Eight iodine ions were arranged at positions of $(c/2, c/2, 0)$, $(-c/2, c/2, 0)$, $(c/2, -c/2, 0)$, $(-c/2, -c/2, 0)$, $(0, 0, c/2)$, $(0, 0, -c/2)$, $(c, 0, c/2)$ and $(c, 0, -c/2)$, where c is the lattice constant (5.07Å). Positions (x, y, z) of silver ion were varied from 0 to 2.40Å in calculating the shielding values. Step size is 0.20Å for each direction. The schematic complex ion model is formation as shown in Fig.3.7.

A part of the calculation result is shown in Fig.3.8. This figure shows a contour plot of the Ag chemical shielding surface on (001) plane of the α-AgI crystal. The iodine atoms were fixed at four corners in the figure. The figure indicated that the shielding in the octahedral 6(b) and tetrahedral 12(d) sites were comparable and high values, in other words, the shifts were lower field. In vicinities of the trigonal 24(h) site, the shift was the highest field. The calculated values in three sites were listed in Table 3.3. The calculated chemical shifts were dominated by the paramagnetic term similar to our previous investigation [23], since the diamagnetic terms were almost constant (4678±1ppm).
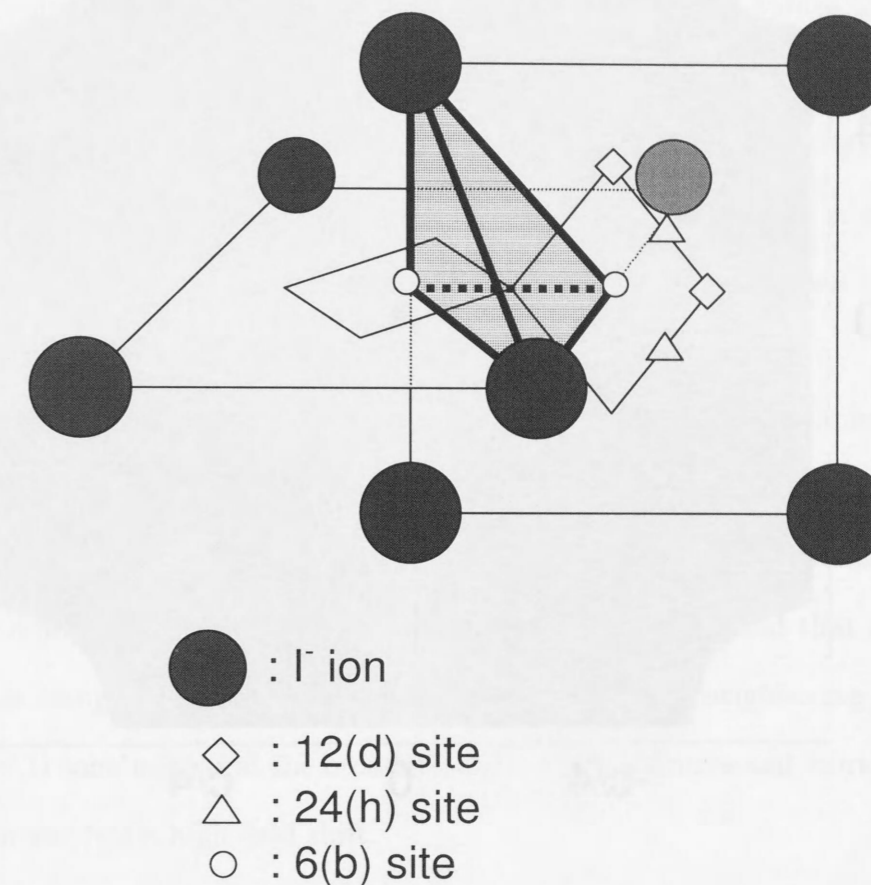
Figure 3.7: The schematic complex ion model $[AgI_8]^{7-}$. Solid circles (•) denote the positions of the iodine ions and the shaded area indicates the space in which Ag$^+$ ions are located. ◇, △ and ○ denote the 12(d), 24(h) and 6(b) sites for the cation, respectively.
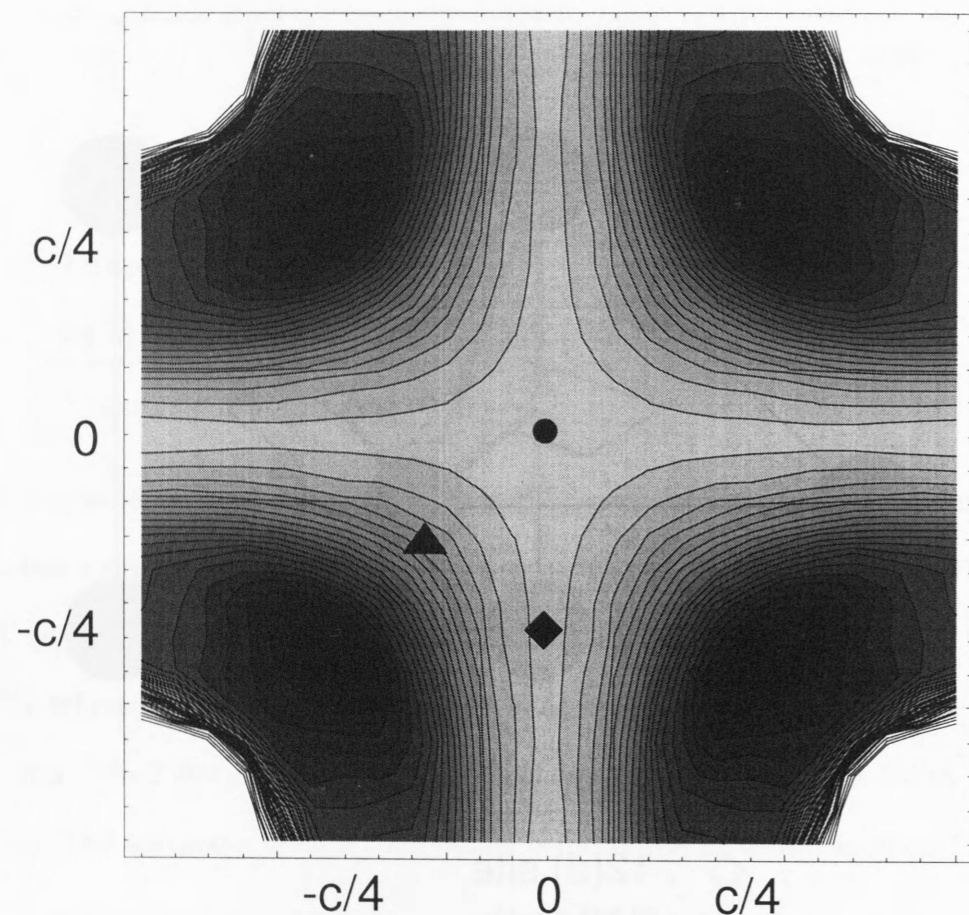
Figure 3.8: Contour plot of the Ag chemical shielding surface on (001) plane of the α-AgI crystal. Shielding value in the dark place gives the high field shift. Contour interval is 30ppm. c denote a lattice constant (5.07Å). $\diamondsuit$, $\triangle$ and $\bigcirc$ denote the 12(d), 24(h) and 6(b) sites, respectively.

3.3.3   Average shielding value

The average shielding values at each temperature were calculated by the sum of convolutions of the density set and the shielding surface in Eq.(3.7). The calculated Ag chemical shifts in α-phase were given relative to the reference shielding value at 473K. Comparison between the calculated and the observed values of Ag chemical shifts at 513 and 573K are shown in Fig.3.9. From the figure, the calculated shifts reflected the observed qualitative trend well to the high field in analogy with the case of the γ-phase. The result indicated that the chemical shift in the α-phase could be also explained by using the temperature factor that includes effects of the thermal vibration and the diffusive motion of the mobile ion.

In Table 3.3, the shift of 24(h) site was the highest field in stable sites. So we considered that the temperature dependence of the observed shift was attributable to the increasing density at a vicinity of the 24(h) site, relative to other sites. From the neutron diffraction study [2], Cave and co-workers also described that the increase in density as being caused by the broadening of the density on neighboring 12(d) sites. It, therefore, is concluded that the broadening due to the diffusive and vibrational motions results in the NMR high field shift.

It is a debatable point that the calculated results reproduce only the observed trends of the chemical shift, since the number of the probability densities of Ag atom have been never observed enough to be enabled the quantitative discussion. By classical molecular dynamics (MD) simulations, many studies have ever tried to investigate local structure of the α-AgI crystal. In the next chapter, we will try to calculate the chemical shift by using simulated probability density from the MD method.
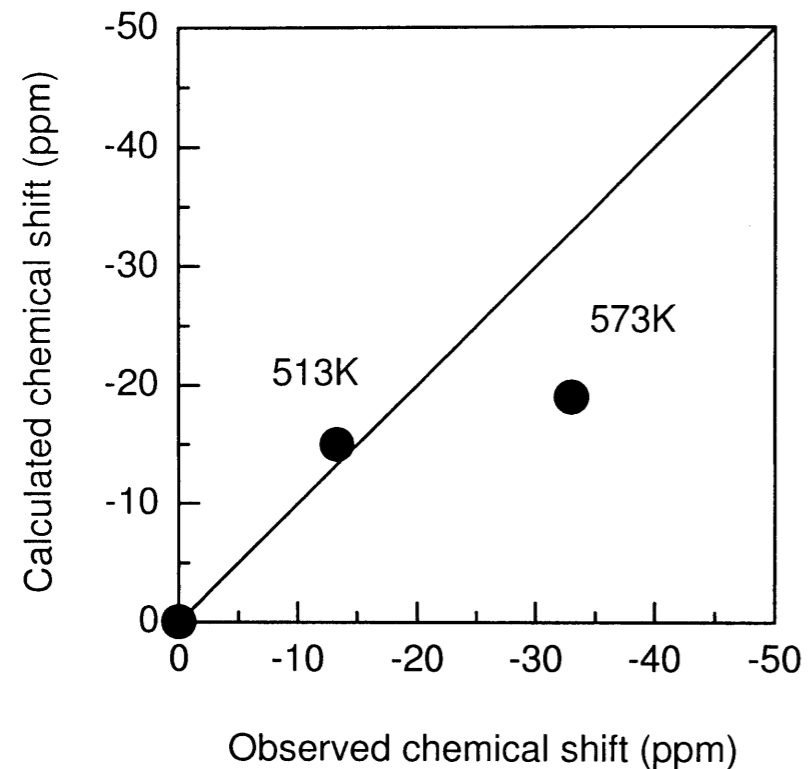
Figure 3.9: Comparison between the calculated and the observed values of Ag chemical shifts at 513 and 573K. The Ag chemical shifts are given relative to the reference shielding value at 473K.

Chapter 4

MO and MD applications to theoretical chemical shift

Some groups of theoretical investigators applied a classical molecular dynamics (MD) method to obtain the microscopic information for α-AgI [12–15]. By using a soft-core potential in the α-AgI system, they simulated the static and dynamic structures to compare with some experimental results. Fukumoto and co-workers described that the Ag^{+} ions were preferentially distributed in oblong elliptic regions centered in the vicinity of the 12(d) sites [12]. In the other MD work, Hokazono and Ueda showed a diffusion process of Ag^{+} ion that was continuous jumping from one 12(d) site to nearest-neighbor (n.n.) 12(d) sites [14]. Although the MD simulations explained the dynamical information for α-AgI in detail, no studies have ever been tried to apply the MD method to illustrate the NMR spectral results which gave much detailed microscopic dynamical structures, selectively.

In the present chapter, we will show the chemical shift calculations using the MD simulation for the α-AgI. As mentioned in previous chapter, the average shielding value

is calculated by the sum of convolution of the shielding surface and the probability density of the mobile ion. The probability density is estimated by the MD simulation in this chapter. The dynamical structure of the mobile ion in the α-AgI will be discussed by comparing the observed and the calculated chemical shift. Furthermore the ^{63}Cu NMR chemical shifts for $Ag_{0.99}Cu_{0.01}I$ crystal is measured over the temperature range between 295K and 520K (γ- to α-phase). The experimental results of ^{63}Cu NMR chemical shifts will be also analyzed by using both the Cu NMR chemical shielding surface and the probability density of the cation.

4.1   Chemical shift for α-AgI using MD simulation

In the analogy of previous chapter, we supposed that the density of atom at temperature T can be written as $\rho(\mathbf{R}, T)$, then the average shielding value ($\sigma^{\text{ave}}(T)$) is expressed as

$$\sigma^{\text{ave}}(T) = \sum_{i,j,k}^{\text{unit}} \sigma(x_i, y_j, z_k) \times \rho(x_i, y_j, z_k, T) \,. \tag{4.1}$$

where the sum is over the range of one unit lattice in the crystal. Thus, we calculated the shielding surface and the probability density of the cation by using the methods as described in computational section.

4.1.1   Computational details

The shielding values were calculated on the basis of the ab initio MO method. Isolated complex ion $[AgI_8]^{7-}$ was employed to the model of α-AgI crystal. Eight iodine ions were arranged at positions of $(c/2, c/2, 0)$, $(-c/2, c/2, 0)$, $(c/2, -c/2, 0)$, $(-c/2, -c/2, 0)$, $(0, 0, c/2)$, $(0, 0, -c/2)$, $(c, 0, c/2)$ and $(c, 0, -c/2)$, where c was the av-

erage lattice constant that was estimated as 4.90Å by the present MD simulation of α-AgI. Positions (x, y, z) of copper ion were varied from 0 to 2.40Å in calculating the shielding values. Step size is 0.20Å for each direction. The schematic complex ion model is shown in Fig.3.7. The basis sets used for Ag and I atoms were DZVP [38] and LANL2DZ [46], respectively. The calculations of the chemical shielding value were carried out with Gaussian 98 [47].

The molecular dynamics (MD) calculation using ionic potential (*soft-core potential*) was well employed to many ionic materials [10–12]. The potential was given by

$$\phi_{ij}(r) = \varepsilon \left(\frac{\pi_i + \pi_j}{r} \right)^n + \frac{Z_i Z_j (fe)^2}{r} \,, \tag{4.2}$$

where π_i and Z_i were the effective core radius and valency of ion i, respectively. Here the ionicity f was also introduced. The computation was carried out with total ion number N = 500 in the temperature range of 500 to 600K. Initially, 250 iodine ions were in the *bcc* arrangement, while 250 silver-ions were distributed at random in the tetrahedral 12(d) positions. In this calculation, we chose $\pi_I = 2.20$Å, $\pi_{Ag} = 0.63$Å, $n = 7$ and $f = 0.6$, as discussed by Vashishta and Rahman [9]. We also used the repulsion parameter, $\varepsilon = 0.0851$eV by Kaneko and Ueda [15], and evaluated the coulomb terms by the Ewald method [48]. The equations of motion were integrated up to 500,000 time steps by Verlet's algorithm [49], where we started the sampling after the initial 10,000 time steps running; one time step being 9.28fs. The MD calculation techniques in detail are shown in Appendix B. All sampled particles were determined a relative position to the bcc lattice of the iodines. The one unit bcc lattice was separated 25 × 25 × 25 partitions, whose one side was 0.2Å, and the probability density is evaluated by counting particles in one partition.

Table 4.1: Calculated Ag chemical shielding values at the 6(b), 12(d) and 24(h) sites. The chemical shifts are given relative to the shielding value in the 12(d) site.

site	σ_{dia} (ppm)	σ_{para} (ppm)	σ_{total} (ppm)	shift (ppm)
6(b)	4680	-1231	3448	29
12(d)	4678	-1259	3419	0
24(h)	4680	-1345	3335	-84

4.1.2 Results

The Ag chemical shielding surface on (001) plane was a similar tendency to the calculated one in the preceding chapter (see Fig.3.8). The calculated values in each site are listed in Table 4.1. The calculated chemical shift was also dominated by the paramagnetic term similar to our previous investigation [23], since the diamagnetic terms are almost constant (4679±1ppm).

Fig.4.1 shows a contour plot of the Ag probability density on (001) plane obtained by the MD simulation at 500K. These results corresponded well to the experimental ones for the Ag probability density determined by neutron diffraction method [2]. The density of cation mainly located at the 12(d) sites and together with some densities at the 24(h) and the 6(b) positions.

The average shielding values was calculated by the sum of convolutions of the Ag chemical shielding surface and the probability density of the cation. The calculated Ag chemical shifts were given relative to the reference shielding value at 500K. Fig.4.2 shows the comparison between the calculated and the observed values [18] of ^{109}Ag
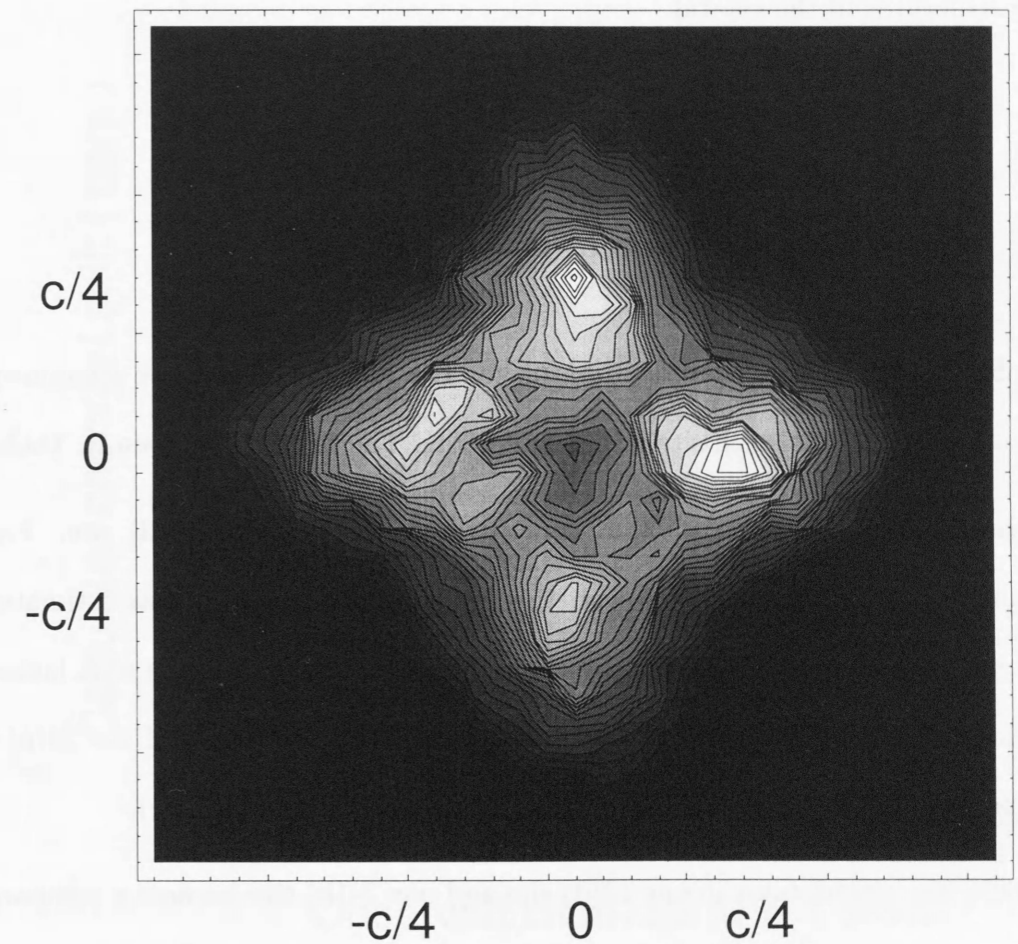

Figure 4.1: Contour plot of the Ag probability density on (001) plane of the AgI crystal at 500K. Light place indicates the area of the high-density value. c denote a lattice constant.

chemical shift for α-AgI in the temperature range of 500 to 600 K. The calculated shift was in good agreement with the observed one. It was clear that the average shielding value from the MD calculations should provide the temperature dependence of the chemical shift for α-AgI. In addition, the MD simulation present a great information of local structures in the crystal.

4.1.3   Population analysis in stable sites

In order to clarify the theoretical reason for the high field shift, we examined the change of the density at each site at 500 and 600K. The results are given in Table 4.2.

The population of cations at 500K concentrated surely in the 12(d) site. From a viewpoint of one unit lattice, however, the total population, that was estimated by multiplying the one site population by the numbers of the site in one unit lattice, in the 24(h) sites was the greatest in the stable site, since the number of the 24(h) sites in one unit lattice is the greatest number (24 sites per one unit lattice).

At 600K, the populations in one 12(d) site and one 24(h) site became a comparative value. It seems that the comparative population came from a very fast jumping rate ($> 10^{12}$ /s) of the mobile ions between the 12(d) and 24(h) sites from motional analysis in the MD simulation. As a result, the total population in the 12(d) site relatively decreased. It, therefore, was concluded that the chemical shift was mainly influenced by an electronic structure of cations at the 24(h) site and the shieldings shifted to the higher field than that at 500K.

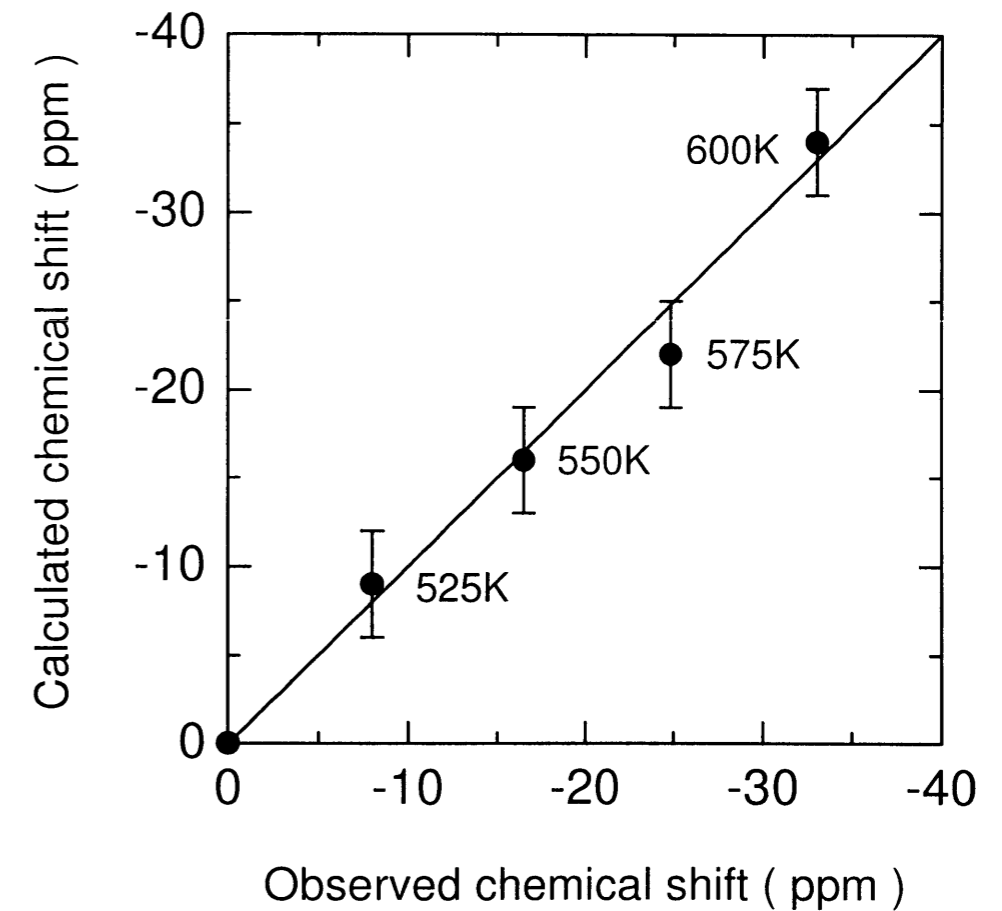The motional analysis of the mobile ion will be discussed in detail in the next chapter.

Figure 4.2: Comparison between the calculated and the observed values of ^{109}Ag chemical shift for α-AgI in the temperature range of 500 to 600 K.

Table 4.2: Temperature dependence of population ($\rho(R, T)dv^*$) in the 6(b), 12(d) and 24(h) sites at 500K and 600K. Total populations are calculated by multiplying the one site population by the numbers of the site in one unit lattice.

site	population 500K		population 600K	
	one site	total	one site	total
	($\times 10^{-4}$)	(%)	($\times 10^{-4}$)	(%)
6(b)	1.79	0.11	3.25	0.20
12(d)	4.00	0.48	2.61	0.31
24(h)	2.76	0.66	2.79	0.67

* : $dv = 8.0 \times 10^{-3} \text{Å}^3$

4.2 ^{63}Cu NMR chemical shift in α-Ag$_{0.99}$Cu$_{0.01}$I

The temperature dependence of Ag chemical shift in the α-AgI was produced by considering the average shielding value. The observed temperature dependence (- 0.33ppm/K) was, however, determined by measurements at three temperature points [18], since one could scarcely observe the solid ^{109}Ag NMR signal in the superionic phase owing to its extremely low intensity and very long spin-lattice relaxation time. So, we will try to measure the temperature dependence of ^{63}Cu chemical shift in α-Ag$_{0.99}$Cu$_{0.01}$I instead of α-AgI, and calculate the average shielding value for Cu atom.

4.2.1 Experimental procedures

We used the commercially available AgI and CuI reagents. The Ag$_{0.99}$Cu$_{0.01}$I crystal in the complete solid solution was prepared by the melt annealing method in a nitrogen

gas to prevent oxidation.

Solid ^{63}Cu NMR measurements of Ag$_{0.99}$Cu$_{0.01}$I were performed at a frequency of 79.12MHz, using a Chemagnetics CMX-300 spectrometer. 128 transients were accumulated using a 4.9 - 9.5μs (90°) pulse. The spectra were obtained under the magic-angle spinning at a speed of about 3.0kHz; and 8k data points were collected over bandwidths of 650kHz. All measurements were carried out over the temperature range of 295 520K.

^{63}Cu NMR chemical shift in Ag$_{0.99}$Cu$_{0.01}$I at 295K was used as an external reference. All chemical shifts for ^{63}Cu are defined by

$$\sigma^{\text{exp}} = \frac{\nu_{\text{sam}} - \nu_{\text{ref}}}{\nu_{\text{ref}}}, \tag{4.3}$$

where ν_{sam} is the resonance frequency of the sample and ν_{ref} is the reference frequency; the shift defined in this manner was negative for higher field shift.

Fig.4.3 shows the temperature dependence of the ^{63}Cu chemical shift observed in the range of 295 - 520K. The signals shifted to the high field with increasing temperature in both γ- and α-phases. In the figure, we can see a discontinuity between the γ- and α-phases in the transition temperature range of 440 $\sim$ 450K indicating the first order phase transition, and can obtain the similar slopes of -0.2 ppm/K in both phases.

4.2.2 Cu average shielding value for Ag$_{0.99}$Cu$_{0.01}$I

For the α-Ag$_{0.99}$Cu$_{0.01}$I , the shielding surface was calculated by the same methods in the α-AgI with the exception of the model molecule. The isolated complex ion [CuI$_8$]$^{7-}$ was employed to the model of α-Ag$_{0.99}$Cu$_{0.01}$I crystal.

Fig.4.4 shows a contour plot of the Cu chemical shielding surface on (001) plane of the Ag$_{0.99}$Cu$_{0.01}$I crystal. The iodine atoms were fixed at four corners in the figure.

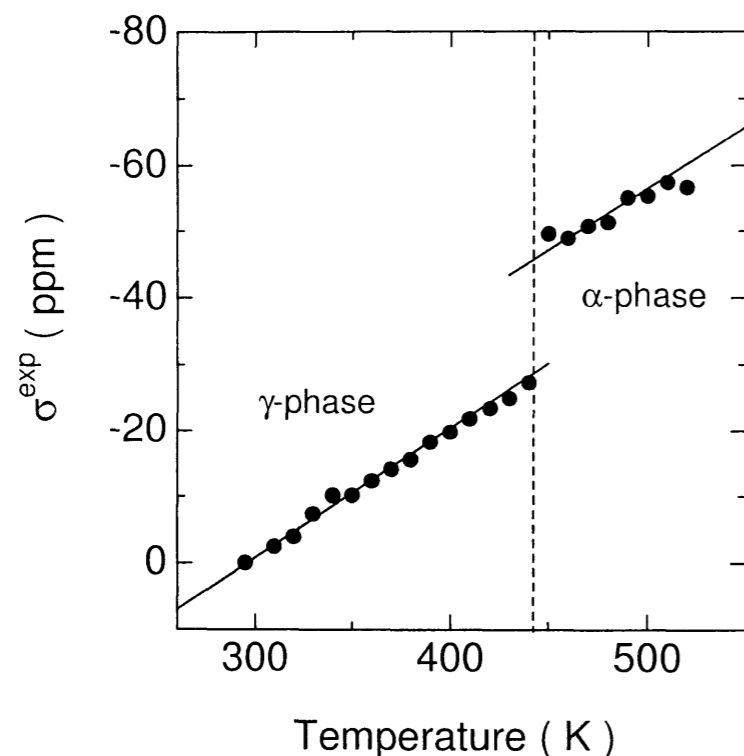**Figure 4.3:** Temperature dependence of ^{63}Cu NMR chemical shift. ^{63}Cu NMR chemical shift in Ag$_{0.99}$Cu$_{0.01}$I is used as an external reference at 295K.

Table 4.3: Calculated Cu chemical shielding values at the 6(b), 12(d) and 24(h) sites. The chemical shifts are given relative to the shielding value in the 12(d) site.

site	σ_{dia} (ppm)	σ_{para} (ppm)	σ_{total} (ppm)	shift (ppm)
6(b)	2408	-535	1873	59
12(d)	2404	-591	1814	0
24(h)	2407	-620	1787	-27

While the shielding value in the octahedral 6(b) site was the highest; in other words, the shift was the lowest field, in vicinities of the trigonal 24(h) site, the shift was the highest field as similar to the case of Ag shielding surface in the preceding section. The calculated values in each site are listed in Table 4.3. The calculated chemical shift was also dominated by the paramagnetic term similar to our previous investigation [23], since the diamagnetic terms are almost constant (2406±2ppm).

The average shielding values was estimated by the sum of convolutions of the Cu chemical shielding surface and the probability density of the cation. The calculated Cu chemical shifts were given relative to the reference shielding value at 500K. Fig.4.5 shows the comparison between the calculated and the observed values of ^{63}Cu chemical shift for α-Ag$_{0.99}$Cu$_{0.01}$I in the temperature range of 500 to 600 K. The calculated shift was in good agreement with the observed one. It was concluded that the combined use of the shielding surfaces from the ab initio MO calculation and the probability density from the MD simulation should provide a useful way of local structure analysis for Ag$_X$Cu$_{1-X}$I crystal.
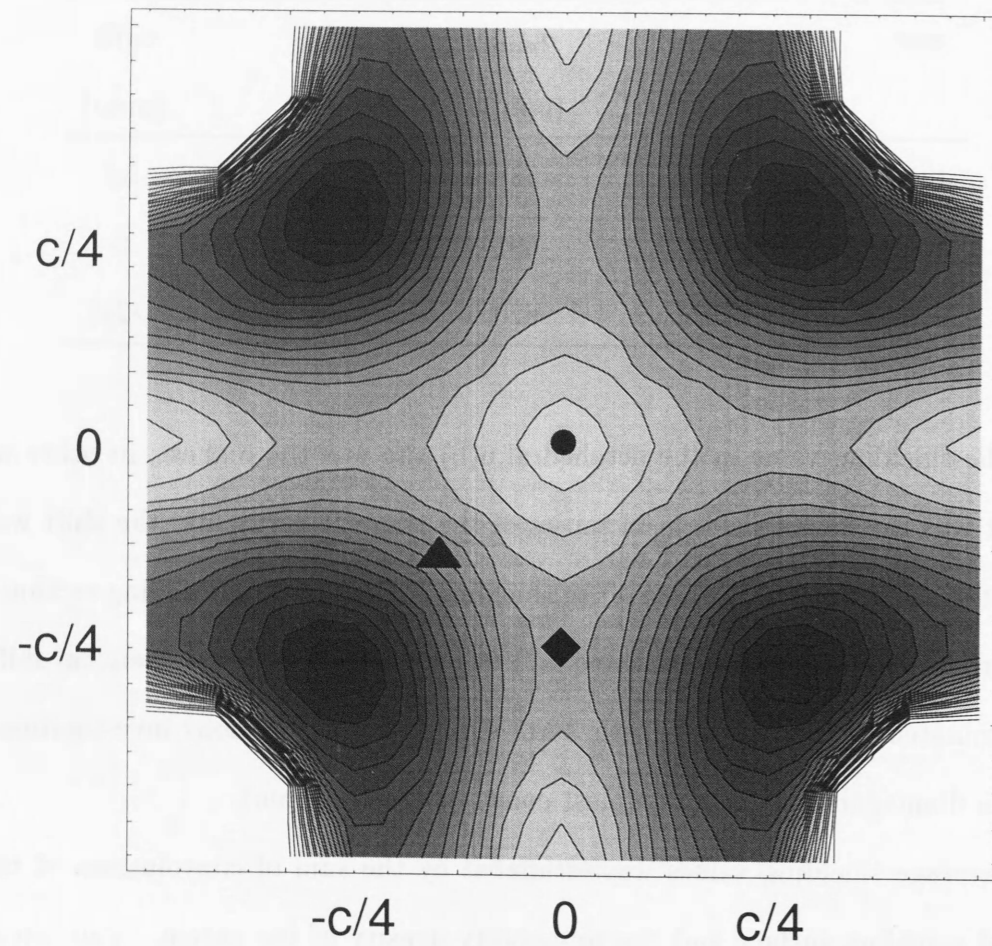
Figure 4.4: Contour plot of the Cu chemical shielding surface on (001) plane of the Ag$_{0.99}$Cu$_{0.01}$I crystal. Shielding value in the dark place gives the high field shift. Contour interval is 20ppm. c denote a lattice constant. $\diamondsuit$, $\triangle$ and $\bigcirc$ denote the 12(d), 24(h) and 6(b) sites for the cation, respectively.

Figure 4.5: Comparison between the calculated and the observed values of ^{63}Cu chemical shift for α-Ag$_{0.99}$Cu$_{0.01}$I in the temperature range of 500 to 600 K.

Chapter 5

Spin-lattice relaxation by MD simulation

We have discussed the relation between the metal chemical shift and the local structure in $Ag_xCu_{1-x}I$ crystal from γ- to α-phase. In this chapter, we will clarify the dynamical diffusion process of the cation in the α-phase from an analysis of NMR spin-lattice relaxation time.
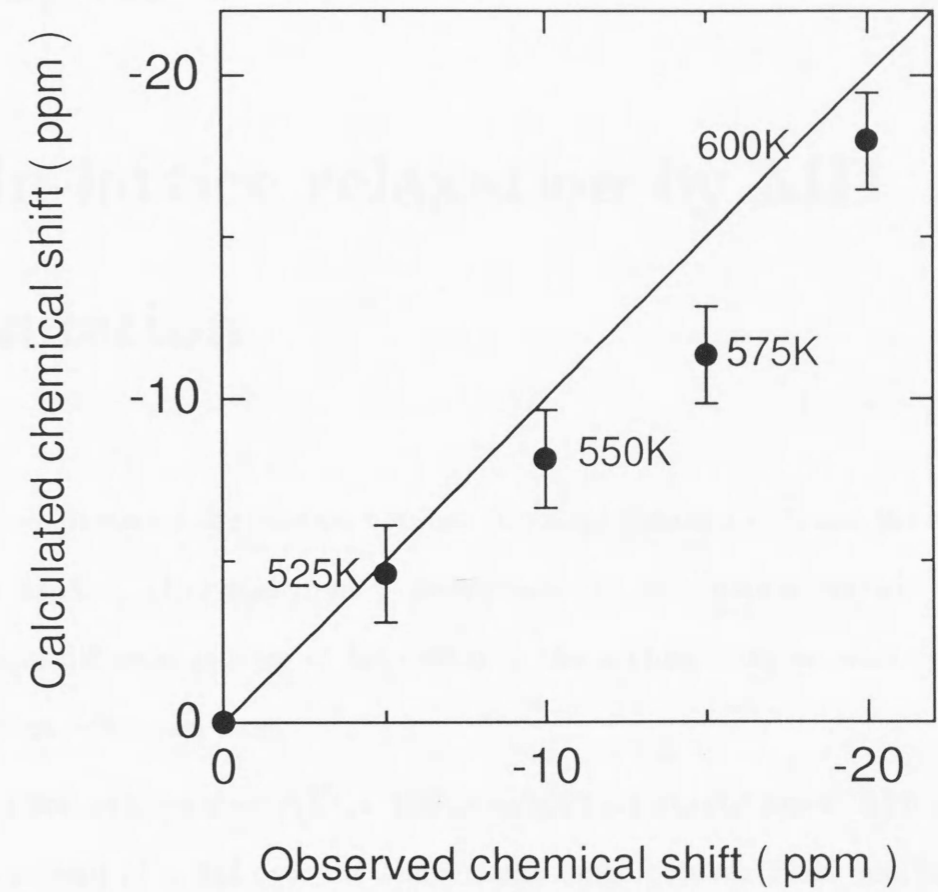
In the first step, we observe [63]Cu NMR spin-lattice relaxation times (T_1) for $Ag_{0.99}Cu_{0.01}I$ crystal instead of α-AgI over the temperature range between 295K and 520K (γ- to α-phase). The temperature dependence of the spin-lattice relaxation times will be also analyzed by the MD method.

If there is no way of calculating the correlation function, one has to be satisfied with phenomenological interpretations of the raw data. For instance, an obvious extension of the Bloembergen-Purcell-Pound model [50] is the assumption that instead of one process a distribution of jumping processes exists. Walsted and co-workers introduced this model to NMR studies in Na β-almina as SIC [51]. The MD simulation, however,

directly provides us the distribution of the jumping process, and the correlation function

becomes feasible to calculate by the distribution.

5.1 ^{63}Cu NMR T_1 in Ag$_{0.99}$Cu$_{0.01}$I

We used the commercially available AgI and CuI reagents. The Ag$_{0.99}$Cu$_{0.01}$I crystal

in the complete solid solution was prepared by the melt annealing method in a nitrogen

gas to prevent oxidation.

Solid ^{63}Cu NMR measurements of Ag$_{0.99}$Cu$_{0.01}$I were performed at a frequency of

79.12MHz, using a Chemagnetics CMX-300 spectrometer. 128 transients were accumu-

lated using a 4.9 - 9.5μs (90°) pulse. The spectra were obtained under the magic-angle

spinning at a speed of about 3.0kHz; and 8k data points were collected over bandwidths

of 650kHz. All measurements were carried out over the temperature range of 295 –

520K. ^{63}Cu NMR spin-lattice relaxation time (T_1) was measured using a $180° - \tau - 90°$

pulse sequence. The error in the T_1 measurements was estimated to be ± 10%.

Figs.5.1 shows the temperature dependence of ^{63}Cu NMR spin-lattice relaxation time

(T_1) in Ag$_{0.99}$Cu$_{0.01}$I crystal in the range of 295 – 520K. In the γ-phase, the T_1 decreased

gradually with increasing temperature below 380K. This result was owing to the lattice

vibration. Over the temperature range of 380 - 440K, it could be seen a sudden change

of T_1 owing to the first order structural phase transition of the Ag$_{0.99}$Cu$_{0.01}$I crystal.

In the α-phase (Fig.5.1(b)), T_1 increased with increasing temperature above 450K.

The temperature dependence of T_1 in the α-phase is explained by the Arrhenius

relation, since the relaxation in the superionic conductor is dominated by fast diffusive

motion where cations are jumping among the stable sites. We obtained the activation

energy of the Cu$^+$ ion diffusion as $E_a = 11$ kJ/mol. This activation energy was consid-
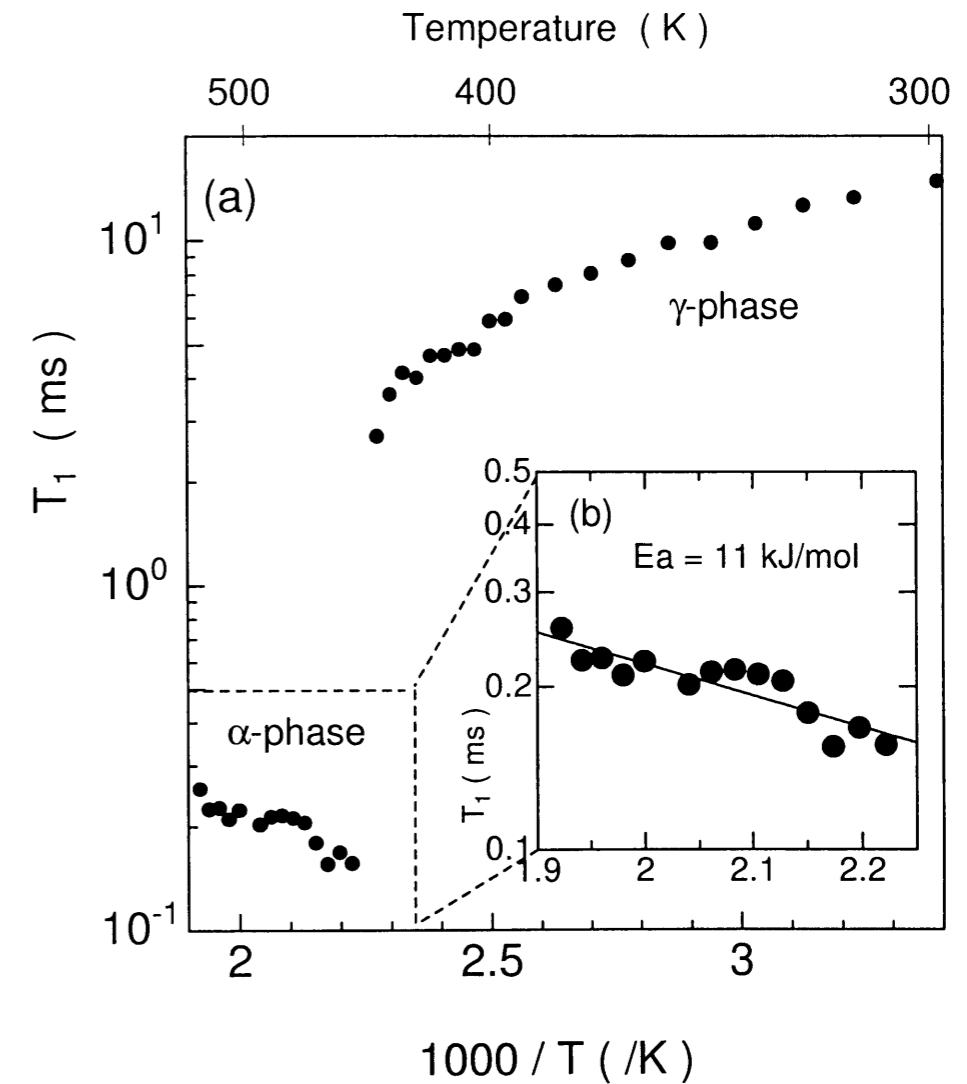
Figure 5.1: Temperature dependence of ^{63}Cu NMR spin-lattice relax-
ation time observed in Ag$_{0.99}$Cu$_{0.01}$I .

ered to be a barrier height for a jumping of the mobile (copper and silver) ions between sites in the bcc lattice.

5.2 T_1 by jumping model

While normal phonon contributions to the spin-lattice relaxation time (T_1) may be present, the nuclear relaxation in α-$Ag_{0.99}Cu_{0.01}I$ is clearly dominated by the diffusive motion, i.e., by the interaction of fluctuating electric-field-gradient (EFG) with the nuclear quadrupole moments. We specialize our discussion of quadrupolar relaxation to the case of $I = 3/2$ (^{63}Cu). In an applied field H_0 we have four splitting energy levels E_m ($m = \pm 3/2, \pm 1/2$) and the nuclear quadrupolar coupling gives rise to averaged shifts and transitions among the levels E_m caused by the fluctuating part of the interaction term.

$$\mathcal{H}_Q = \sum_i \sum_{M=1}^{2} [A_M(\mathbf{I}_i) V_{iM}(t)], \tag{5.1}$$

where subscripts i, and M stand for the ith nucleus, and (first or second)-order transition, respectively. $A_M(\mathbf{I}_i)$, and $V_{iM}(t)$ denote the Mth-order quadrupolar moment term and the time-dependent EFG tensor at the ith nucleus, respectively.

The T_1 is generally expressed by the time-dependent perturbation method, as follows:

$$\begin{aligned} T_1^{-1} &= \sum_{m,m'} \sum_i \sum_{M=1}^{2} |\langle m|A_M|m'\rangle|^2 \\ &\times \int d\tau \, \exp(i\omega_{m,m'}\tau)\langle V_{iM}(t) V_{iM}^*(t-\tau)\rangle \end{aligned} \tag{5.2}$$

where $\langle V_{iM}(t) V_{iM}^*(t-\tau)\rangle$ is a spin-EFG correlation function for a possible environment in which nucleus i finds itself during the relaxation process.

For the jumping model we neglect the transit time, because the time is much less than 10^{-13}s. We consider that there are random orientations of spins in the stable

sites, and the correlation function will be thus written in terms of both an averaged EFG tensor and a correlation time function ($f(\tau)$),

$$\langle V_{iM}(t) V_{iM}^*(t-\tau)\rangle = \overline{|V_{iM}|^2} \cdot f(\tau) \tag{5.3}$$

We can regard the correlation time as a resident time of a mobile ion i in one site. The correlation function is usually defined as a single exponential function with an averaged correlation time (τ_c), $f(\tau) = \exp(-\tau/\tau_c)$, Walstedt and co-workers defined the correlation time as the function with a distribution of an activation energy, since there was no way of directly calculating the correlation function [51]. For the present, by taking into account the resident times of mobile ions in the MD simulation, it was found that the correlation time has a distribution with a finite width. We, thus, give an assumption of the correlation function by the convolution of the distribution and the exponential functions as,

$$f(\tau) = \int_0^\infty d\tau_r \, \mathcal{D}(\tau_r) \exp\left(-\frac{\tau}{\tau_r}\right) \tag{5.4}$$

where $\mathcal{D}(\tau_r)$ is the normalized distribution function of resident times. If the distribution is given by the Dirac's delta function without a finite width, then the correlation function becomes a single exponential correlation function in the BPP equation [50]. The assumption in this jumping model, therefore, is understood as an obvious extension of the BPP model.

We make an assumption to consider the transition of only $m' = m \pm 1$. By using Eqs.(5.2), (5.3) and (5.4), we obtain the following expression for T_1,

$$\begin{aligned} T_1^{-1} &= \sum_m \sum_i \sum_M |\langle m|A_M|m \pm 1\rangle|^2 \\ &\times \int d\tau \, \exp(i\omega\tau)\overline{|V_{iM}|^2} \int_0^\infty d\tau_r \, \mathcal{D}(\tau_r) \exp\left(-\frac{\tau}{\tau_r}\right) \end{aligned}$$

$$= \overline{|R_1|^2} \int_0^\infty d\tau_r \, \mathcal{D}(\tau_r) \frac{2\tau_r}{1 + (\omega\tau_r)^2} \qquad (5.5)$$

where

$$\overline{|R_1|^2} = \sum_m \sum_i |\langle m|A_1|m \pm 1\rangle|^2 \overline{|V_{i1}|^2} \,.$$

The final equation is employed to analyze the spin-lattice relaxation time in the jumping model. In the equation, it is needed only the information of the distribution function for the resident time ($\mathcal{D}(\tau_r)$). The MD method yields directly the information on the time and position of the mobile ions in the α-AgI.

Hokazono and Ueda [14] described by the MD simulation that mobile Ag ions jumped rapidly into n.n. 12(d) sites in their successive movements. Although they determined the diffusive motion from a sign of the velocity auto-correlation function of ions due to events of pass through and of no-pass through, the NMR experiment is not able to separate the events of pass through and no-pass through. We, therefore, propose two type models for the diffusion process of the mobile ions in order to simulate the NMR relaxation results; (I) 12(d) jumping model is defined a mobile ion jumping from a tetrahedral 12(d) intrasub-lattice to the nearest neighbor (n.n.) 12(d) sub-lattices, where the tetrahedral 12(d) sub-lattice is formed by four anions and a center of this sub-lattice is the 12(d) site. (II) 6(b) jumping model is from an octahedral 6(b) intrasub-lattice, that is formed by six anions, to the n.n. 6(b) sub-lattices.

5.2.1   Distribution of correlation time

We numbered all the sub-lattices and examined the number of the sub-lattice including the Ag$^+$ ion. The resident time of Ag$^+$ ion was determined a time-interval between two adjacent discontinuities on the number line. Similar to the case of calculating the
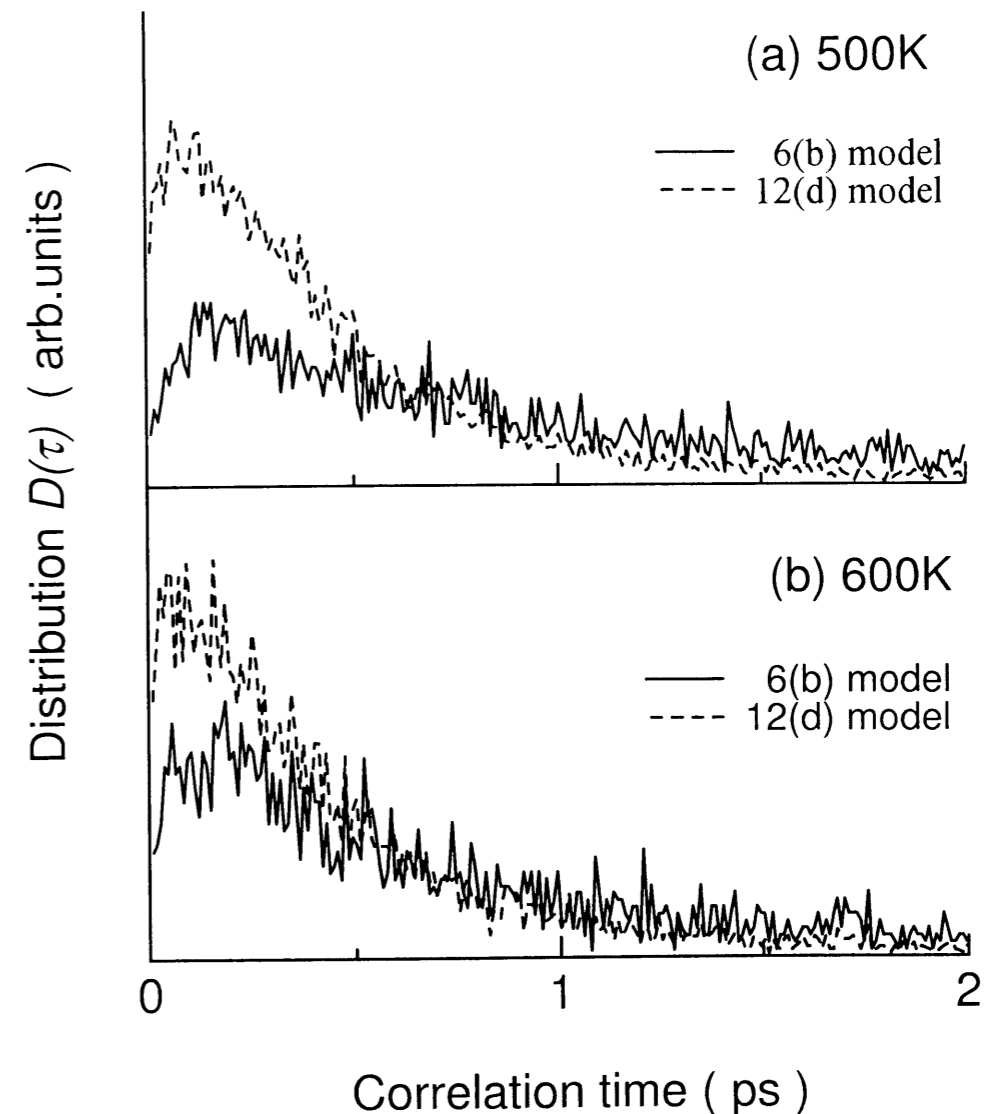
Figure 5.2: Calculated distribution of the resident time of Cu$^+$ ion at (a) 500K and (b) 600K. The solid and broken lines correspond to the 6(b) and 12(d) model, respectively.

probability density in the preceding chapter, the resident time (τ_r) of Ag^+ ion can be regarded as the correlation time of Cu^+ ions in the corresponding sites. Figs.5.2 shows the distribution curve of τ_r in both the 12(d) and 6(b) jumping models at 500 and 600K. The most of mobile ions diffused very quickly through the bcc lattice of iodine, since curves in both models had a peak at about $0.1 \sim 0.2ps$. In the 12(d) model, the distribution curve decreased rapidly from the peak position, while in the 6(b) model the curve gradually decreased with a long tail down to 10ps. So it was estimated the populations of correlation times at more than 1.0ps, as listed in Table 5.1. At 500K the populations in the 12(d) and the 6(b) models were 13% and 45%, respectively. This difference indicated that the jumping rate among the 12(d) sites was mainly more than $10^{12}/s$ and among the 6(b) sites was $10^{12} \sim 10^{10}/s$. Furthermore, the populations in the 12(d) model were independent of temperature and in the 6(b) model decreased with rising temperature.

5.2.2   Activation energy

It was calculated the spin-lattice relaxation times from Eq.(5.5). As an example, Fig.5.3 shows the temperature dependence of the calculated T_1 in $\overline{|R_1|^2}$ unit in the 6(b) model. The activation energy E_a in the 6(b) jumping model was estimated as 9.4 kJ/mol.

In Table 5.1, we summarized the activation energies of the cation in the 12(d) and 6(b) models. The activation energy in the 6(b) model was in good agreement with the observed value. Therefore it was concluded for the relaxation mechanism in $Ag_{0.99}Cu_{0.01}I$ crystal that the observed diffusion process was due to the mobile ion jumps from the octahedral 6(b) intrasub-lattice to the n.n. 6(b) sub-lattices
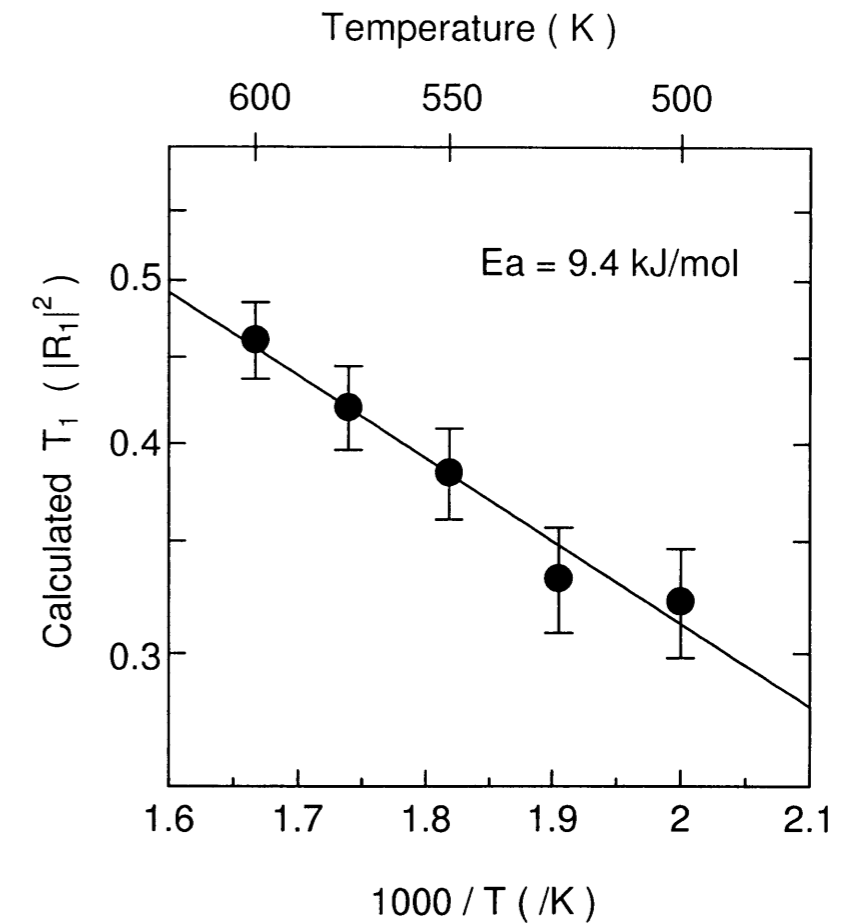
Figure 5.3: Temperature dependence of the calculated ^{63}Cu NMR spin-lattice relaxation time in the 6(b) model. The unit is $|R_1|^2$.

Table 5.1: Estimated the activation energies (E_a) of the cation and the population in the resident time of more than 1.0ps at 500 and 600K, with the observed activation energy by the analysis of the ^{63}Cu NMR measurement.

models	population		E_a
	500K (%)	600K (%)	(kJ/mol)
12(d)	13	13	<0.1
6(b)	45	34	9.4
Obsd.			11

($\tau_r = 10^{-12} \sim 10^{-10}$s). The activation energy in the 12(d) model was too low to reproduce the observed one. This reason was considered that the correlation time for the jumping among 12(d) sites was too fast to contribute the temperature dependence of the NMR spin-lattice relaxation.

In this chapter, we employed the distribution of the correlation time, $\mathcal{D}(\tau_r)$, on the basis of the MD simulation. The NMR T_1 was found to reflect the present of the distribution for ionic motion in α-phase and the MD methods provided a rough but effective probe of its profile when interpreted with NMR spectra.

Chapter 6

Concluding remarks

In this study, we have investigated the local structure of the $Ag_XCu_{1-X}I$ crystal by means of NMR, ab initio MO and MD methods as follows; first, in $Ag_XCu_{1-X}I$ crystals (X=0.0, 0.25, 0.5, 0.75 and 1.0), the observed chemical shieldings were analyzed on the basis of the Ag and Cu NMR shielding calculations of tetrahedral MI_4^{3-} (M = Ag, Cu) ions using the ab initio MO program. The results indicated that the X dependence of the chemical shift was related the bond length between the metal and iodine, and the shift was explained dominantly based on the paramagnetic shielding term, which depended on the d-hole and p-electron densities of the Ag or Cu atom.

Second, according to the chemical shift calculation using the model molecule in equilibrium geometries, the temperature dependence of the calculated chemical shift in the AgI crystal were not in good agreement with the observed high field shift. So we introduced an idea of the average shielding value for calculations of the metal chemical shift. The average shielding value was given by the sum of convolutions of the probability density and the shielding surface of the cation. The results could be reproduced the observed trends of the chemical shift. In the AgI crystal, therefore, it

was clear that the broadening of the cation density due to the diffusive and vibrational motions resulted in the NMR high field shift.

Third, by using the MD simulation for the α-AgI crystal, a number of the probability density were calculated in the temperature range of 500 to 600K. The calculated temperature dependence of the chemical shifts was a pretty good agreement with the observed one. From the analysis of the shielding surface and the density distributions, we concluded that the high field chemical shifts were mainly dominated by the electronic structure of Ag^+ or Cu^+ ions in the 24(h) site.

Finally, the activation energy of Cu^+ ion diffusion in the α-$Ag_{0.99}Cu_{0.01}I$ was estimated as 11kJ/mol from the analysis of the ^{63}Cu NMR T_1 measurement. The temperature dependence of T_1 was simulated by the MD method using the diffusion process in which the cations were jumping of two cases; among octahedral 6(b) sub-lattices and among tetrahedral 12(d) sub-lattices. The calculated results indicated that the diffusion process was mainly due to the cations jumping from the octahedral 6(b) intrasub-lattice to the n.n. 6(b) sub-lattices, since the activation energy in the 6(b) model was in good agreement with the observed value.

In the present work, it should also be emphasized that the combined use of the shielding surfaces from the ab initio MO calculation and the probability density from the MD simulation should provide a useful way of local structure analysis for solid-state compounds. In NMR measurements, this method can be expected to be of most use in situations where there are static and dynamic disordered materials to define structure, or complicated molecules or protein to facilitate structure refinement and validation.

Appendix A

Generalized temperature factor

The Gaussian model of the probability density function $\rho_0(\mathbf{r})$ for atomic thermal motion is adequate in many cases. Where anharmonicity of curvilinear motion is important, however, more elaborate models are needed.

In the classical (high-temperature) regime the generalized temperature factor is given by the Fourier transform of the one-particle probability density function,

$$\rho(\mathbf{r}) = N^{-1} \exp\left[-\frac{V(\mathbf{r})}{kT}\right] \tag{A.1}$$

where

$$N = \int \exp\left[-\frac{V(\mathbf{r})}{kT}\right] d\mathbf{r} \tag{A.2}$$

In the cases where the potential $V(\mathbf{r})$ is a close approximation to the Gaussian (harmonic) potential, series expansions based in a perturbation treatment of the anharmonic terms provide a satisfactory representation of the temperature factors. That is, if the deviations from the Gaussian shape are small, approximations obtained by adding higher-order corrections to the Gaussian model are satisfactory.

In an arbitrary coordinate system the number of significant high-order tensor coefficients for the correction is large. It may be helpful to choose coordinates parallel to the principal axes for the harmonic approximation so that

$$\frac{V(\mathbf{r})}{kT} = \frac{1}{2}\sum_{i=1}^{3}\left(\frac{\mathbf{r}_i}{U_{ii}}\right)^2 \tag{A.3}$$

Eq. (A.1) can be rewritten

$$\rho_0(\mathbf{r}) = N_0^{-1}\exp\left[-\frac{1}{2}\sum_{i=1}^{3}\left(\frac{\mathbf{r}_i}{U_{ii}}\right)^2\right] \tag{A.4}$$

where

$$N_0 = (8\pi^3 U_{11}U_{22}U_{33})^{-1} \tag{A.5}$$

In the Gram-Charlier series expansion [52], the general probability density function $\rho(\mathbf{r})$ is approximated by

$$\rho(\mathbf{r}) = \left[1 - c^j D_j + \frac{c^{jk}}{2!}D_j D_k - \ldots + (-1)^p\frac{c^{jk\ldots\zeta}}{p!}D_\alpha D_\beta\ldots D_\zeta\right]\rho_0(\mathbf{r}) \tag{A.6}$$

The operator $D_\alpha D_\beta\ldots D_\zeta$ is the pth partial (covariant) derivative $\partial^p/\partial\mathbf{r}_\alpha\partial\mathbf{r}_\beta\ldots\partial\mathbf{r}_\zeta$ and $c^{jk\ldots\zeta}$ is a contravariant component are symmetric for all permutations of indices. The first four have three, six, ten, and fifteen unique components for site symmetry 1. The third- and fourth-order terms describe the skewness and the kurtosis of the probability density function, respectively.

The Gram-Charlier series can be followed using general multidimensional Hermite polynomial tensors, defined by

$$^p H_{\alpha\beta\ldots\zeta}(\mathbf{r}) = (-1)^p\exp\left(\frac{\mathbf{r}^j\mathbf{r}^k}{2U_{jk}}\right)D_\alpha D_\beta\ldots D_\zeta\exp\left(-\frac{\mathbf{r}^j\mathbf{r}^k}{2U_{jk}}\right) \tag{A.7}$$

Setting $w_j = \mathbf{r}^k/U_{jk}$ and nothig that $U_{jk} = U_{kj}$ and $w_j w_k = w_k w_j$, the first few general Hermite polynomials may be expressed as

$$^0H(\mathbf{r}) = 1 \tag{A.8}$$

$$^1H_j(\mathbf{r}) = w_j \tag{A.9}$$

$$^2H_{jk}(\mathbf{r}) = w_j w_k - U_{jk}^{-1} \tag{A.10}$$

$$^3H_{jkl}(\mathbf{r}) = w_j w_k w_l - w_j U_{kl}^{-1} - w_k U_{lj}^{-1} - w_l U_{jk}^{-1}$$

$$= w_j w_k w_l - 3w(_j U_{kl}^{-1}) \tag{A.11}$$

$$^4H_{jklm}(\mathbf{r}) = w_j w_k w_l w_m - 6w(_j w_k U_{lm}^{-1}) + 3U_j^{-1}(_k U_{lm}^{-1}) \tag{A.12}$$

Indices in parentheses indicate terms to be averaged over **all** unique permutations of those indices.

The final expression of the Gram-Charlier series is then

$$\rho(\mathbf{r}) = \rho_0(\mathbf{r})\left[1 + \frac{1}{3!}c^{jkl}H_{jkl}(\mathbf{r}) + \frac{1}{4!}c^{jklm}H_{jklm}(\mathbf{r}) + \ldots\right] \tag{A.13}$$

in which the mean and the dispersion of $\rho_0(\mathbf{r})$ have been chosen to make c^j and c^{jk} vanish.

Appendix B

MD calculational techniques

B.1 Ewald method

The Ewald method is a technique for efficiently summing the interaction between an ion and all its periodic images. It was originally developed in the study of ionic crystals [53]. The potential energy can be written as

$$\mathcal{V}^{zz} = \frac{1}{2} \sum_n {}' \left(\sum_{i=1}^{N} \sum_{j=1}^{N} z_i z_j |\mathbf{r}_{ij} + \mathbf{n}|^{-1} \right) \tag{B.1}$$

where z_i, z_j are the charges. The sum over $\mathbf{n}$ is the sum over all simple cubic lattice points, $\mathbf{n} = (n_x L, n_y L, n_z L)$ with n_x, n_y, n_z integers. This vector reflects the shape of the basic box. The prime indicates to omit $i = j$ for $\mathbf{n} = 0$. For long-range potentials, this sum is conditionally convergent, i.e. the result depends on the order in which we add up the terms. A natural choice is to take boxes in order of their proximity to the central box. The unit cells are added in sequence: the first term has $|\mathbf{n}| = 0$; the second term, $|\mathbf{n}| = L$, comprises the six boxes centered at $\mathbf{n} = (\pm L, 0, 0), (0, \pm L, 0), (0, 0, \pm L)$. As we add further terms to the sum, we are building up our infinite system in roughly spherical layers. When we adopt this approach, we

must specify the nature of the medium surrounding the sphere, in particular its relative permittivity (dielectric constant) ϵ_s. The results for a sphere surrounded by a good conductor such as a metal ($\epsilon_s = \infty$) and for a sphere surrounded by vacuum ($\epsilon_s = 1$) are different [54].

$$\mathcal{V}^{zz}(\epsilon_s = \infty) = \mathcal{V}^{zz}(\epsilon_s = 1) - \frac{2\pi}{3L^3}\left|\sum_i z_i \mathbf{r}_i\right|^2 . \qquad (B.2)$$

This equation applies in the limit of a very large sphere of boxes. In the vacuum, the sphere has a dipolar layer on its surface: the last term in Eq.(B.2) cancels this. For the sphere in a conductor there is no such layer. The Ewald method is a way of efficiently calculating $\mathcal{V}^{zz}(\epsilon_s = \infty)$.

At any point during the simulation, the distribution of charges in the central cell constitutes the unit cell for a neutral lattice which extends throughout space. In the Ewald method, each point charge is surrounded by a charge distribution of equal magnitude and opposite sign, which spreads out radically from the charge. This distribution is conveniently taken to be Gaussian,

$$\rho_i^z(\mathbf{r}) = \frac{z_i \kappa^3}{\sqrt{\pi^3}} \exp(-\kappa^2 r^2) \qquad (B.3)$$

where the arbitrary parameter κ determines the width of the distribution, and $\mathbf{r}$ is the position relative to the center of the distribution. This extra distribution acts like an ionic atmosphere, to screen the interaction between neighboring charges. The screened interactions are now short-ranged, and the total screened potential is calculated by summing over all the molecules in the central cube and all their images in the real space lattice of image boxes.

A charge distribution of the same sign as the original charge, and the same shape as the distribution $\rho_i^z(\mathbf{r})$ is also added. This canceling distribution reduces the overall

potential to that due to the original set of charges. The canceling distribution is summed in reciprocal space. In other words, the Fourier transforms of the canceling distributions (one for each original charge) are added, and the total transformed back into real space. There is an important correction: the recipe includes the interaction of the canceling distribution centered at $\mathbf{r}_i$ with itself, and this self term must be subtracted from the total. Thus, the final result is

$$\begin{aligned}
\mathcal{V}^{zz}(\epsilon_s = 1) \;=\; & \frac{1}{2}\sum_i^N \sum_j^N \left(\sum_{|\mathbf{n}|=0}^{\infty} z_i z_j \frac{\mathrm{erfc}(\kappa|\mathbf{r}_{ij}+\mathbf{n}|)}{|\mathbf{r}_{ij}+\mathbf{n}|} \right. \\
& \left. + \frac{1}{\pi L}\sum_{\mathbf{k}\neq 0} z_i z_j \frac{4\pi^2}{k^2}\exp\left(\frac{-k^2}{4\kappa^2}\right)\cos(\mathbf{k}\cdot\mathbf{r}_{ij}) \right) \\
& - \frac{\kappa}{\sqrt{\pi}}\sum_{i=1}^N z_i^2 + \frac{2\pi}{3L^3}\left|\sum_{i=1}^N z_i\mathbf{r}_i\right|^2 .
\end{aligned} \qquad (B.4)$$

Here $\mathrm{erfc}(x)$ is the complementary error function which falls to zero with increasing x. Thus, if κ is chosen to be large enough, the only tem which contributes to the sum in real space is that with $n = 0$, and so the first term reduces to the normal minimum image convention. The second term is a sum over reciprocal vectors $\mathbf{k} = 2\pi\mathbf{n}/L^2$. A large value of κ corresponds to a sharp distribution of charge, so that we need to include many terms in the k-space summation to model it. In the simulation for the α-AgI, the Ewald method was detailed in ref. [48].

B.2   Verlet's algorithm

The most widely used method of integrating the equations of motion is that initially adopted by Verlet [49]. This method is a direct solution of the second-order Newton's motional equation, $m\mathbf{a}_i = \mathbf{f}_i$. The method is based on positions $\mathbf{r}(t)$, accelerations

$\mathbf{a}(t)$, and the positions $\mathbf{r}(t - \delta t)$ from the previous step. The equation for advancing the positions reads as follows,

$$\mathbf{r}(t + \delta t) = 2\mathbf{r}(t) - \mathbf{r}(t - \delta t) + \delta t^2 \mathbf{a}(t) \, . \qquad (B.5)$$

There are several points to note about Eq.(B.5). It will be seen that the velocities do not appear at all. They have been eliminated by addition of the equations obtained by Taylor expansion about $\mathbf{r}(t)$;

$$\begin{aligned}
\mathbf{r}(t + \delta t) &= \mathbf{r}(t) + \delta t \mathbf{v}(t) + \frac{1}{2}\delta t^2 \mathbf{a}(t) + \dots \\
\mathbf{r}(t - \delta t) &= \mathbf{r}(t) - \delta t \mathbf{v}(t) + \frac{1}{2}\delta t^2 \mathbf{a}(t) - \dots
\end{aligned} \qquad (B.6)$$

The velocities are not needed to compute the trajectories, but they are useful for estimating the kinetic energy (and hence the total energy). They may be obtained from the formula

$$\mathbf{v}(t) = \frac{\mathbf{r}(t + \delta t) - \mathbf{r}(t - \delta t)}{2\delta t} \, . \qquad (B.7)$$

Whereas Eq.(B.5) is correct except for errors of order δt^4 (the local error) the velocities from Eq.(B.7) are subject to errors of order δt^2. More accurate estimates of $\mathbf{v}(t)$ can be made, if more variables are stored, but this adds to the inconvenience already implicit in Eq.(B.7), namely that $\mathbf{v}(t)$ can only be computed once $\mathbf{r}(t + \delta t)$ is known. A second observation regarding the Verlet algorithm is that it is properly centered (i.e. $\mathbf{r}(t - \delta t)$ and $\mathbf{r}(t + \delta t)$ play symmetrical roles in Eq.(B.5)), making it time-reversible. Thirdly, the advancement of positions takes place all in one go, rather than in two stages as differently from the standard predictor-corrector. Thus, these advancements make us employ the Verlet's algorithm.

References

[1] M.A. Ratner and A. Nitzan, *Solid State Ionics* **28-30** (1988) 3.

[2] R.J. Cava, F. Reidinger and B.J. Wuensch, *Solid State Commun.* **24** (1977) 411.

[3] J.B. Boyce, T.M. Hayes, W. Stutius and J.C. Mikkelsen Jr, *Phys. Rev. Lett.* **38** (1977) 1362.

[4] R.L. McGreevy and M.A. Howe, *Annu. Rev. Matter Sci.* **22** (1992) 217.

[5] V.M. Nield, D.A. Keen, W. Hayes and R.L. McGreevy, *Solid State Ionics* **66** (1993) 247.

[6] D.A. Keen, V.M. Nield and R.L. McGreevy, *J. Appl. Cryst.* **27** (1994) 393.

[7] W. Schommers, *Phys. Rev. Lett.* **38** (1977) 1536.

[8] W. Schommers, *Phys. Rev.* **B 17** (1978) 2057.

[9] P. Vashishta and A. Rahman, *Phys. Rev. Lett.* **40** (1978) 1337.

[10] J.P. Hansen and I.R. McDonald, *Phys. Rev.* **A 11** (1975) 2111.

[11] M. Amini, D. Finchman and R.W. Hockney, *J. Phys.* **C 12** (1979) 4707.

[12] A. Fukumoto, A. Ueda and Y. Hiwatari, *J. Phys. Soc. Jpn.* **51** (1982) 3966.

[13] M. Parrinello, A. Rahman, P. Vashishta, *Phys. Rev. Lett.* **50** (1983) 11073.

[14] M. Hokazono, A. Ueda, *Solid State Ionics* **13** (1984) 151.

[15] Y. Kaneko, A. Ueda, *Phys. Rev.* **B 39** (1989) 10281.

[16] P.M. Richards, *Topic in Current Physics* **15** (1979) 141, Springer, Berlin.

[17] J.B. Boyce and B.H. Huberman, *Phys. Rep.* **51** (1979) 189.

[18] K.D. Becker and E. Von Goldmmer, *Chem. Phys.* **48** (1980) 193.

[19] H. Nakatsuji, K. Kanda, K. Endo and T. Yonezawa, *J. Am. Chem. Soc.* **106** (1984) 4653.

[20] K. Endo, K. Yamamoto, K. Matsushita, K. Kanda and H. Nakatsuji, *J. Magn. Res.* **65** (1985) 268.

[21] K. Endo, K. Yamamoto, K. Deguchi and K. Matsushita, *Bull. Chem. Soc. Jpn.* **60** (1987) 2803.

[22] K. Endo, T. Ida, J. Kimura, M. Mizuno, M. Suhara and K. Kihara, *Chem. Phys. Lett.* **308** (1999) 390.

[23] T. Ida, K. Endo, M. Suhara, M. Kenmotsu, K. Honda, S. Kitagawa and H. Kawabe, *Bull. Chem. Soc. Jpn.* **72** (1999) 2061.

[24] J. Kimura, T. Ida, M. Mizuno, K. Endo, M. Suhara and K. Kihara, *J. Mol. Struct.* **522** (2000) 61

[25] N.F. Ramsey, *Phys. Rev.* **78** (1950) 699.

[26] L.C. Snyder and R.G. Parr, *J. Chem. Phys.* **34** (1961) 837.

[27] C.C.J. Roothaan, *Rev. Mod. Phys.* **23** (1951) 69.

[28] W.N. Lipscomb, *Advan. Magn. Res.* **2** (1966) 137.

[29] R.M. Stevens, R.M. Pitzer and W.N. Lipscomb, *J. Chem. Phys.* **38** (1963) 550.

[30] R. Ditchfield, in *"International Review of Science: Physical Chemistry"* (A. Allen, ed.) Med. Tech. Press, (1972) New York.

[31] J.A. Pople, J.W. McIver, Jr. and N.S. Ostlund, *J. Chem. Phys.* **49** (1968) 2960.

[32] H.F. Hameka, *Rev. Mod. Phys.* **34** (1962) 87.

[33] F. London, *J. Phys. Radium* **8** (1937) 397.

[34] R. Ditchfield, *J. Chem. Phys.* **56** (1972) 5688.

[35] R. Ditchfield, *Chem. Phys. Lett.* **15** (1972) 203.

[36] J. Kimura, Doctor Thesis, Kanazawa University, (2000) Japan.

[37] M.J. Frisch, G.M. Trucks, H.B. Schlegel, P.M.W. Gill, B.G. Johnson, M.A. Robb, J.R. Cheeseman, T.A. Keith, G.A. Petersson, J.A. Montgomery, K. Raghavachari, M.A. Al-Laham, V.G. Zakrzewski, J.V. Ortiz, J.B. Foresman, J. Cioslowski, B.B. Stefanov, A. Nanayakkara, M. Challacombe, C.Y. Peng, P.Y. Ayala, W. Chen, M.W. Wong, J.L. Andress, E.S. Replogle, R. Gomperts, R.L. Martin, D.J. Fox, J.S. Binkley, D.J. DeFrees, J. Baker, J.P. Stewart, M. Head-Gordon, C. Gonzalez and J.A. Pople, Gaussian 94, Revision C.2, Gaussian, Inc., (1995) Pittsburgh, PA.

[38] N. Godbout, D.R. Salahub, J. Andzelm and E. Wimmer, *Can. J. Chem.* **70** (1992) 560.

[39] E. Clementi, D. L. Raimondi and W. P. Rwinhardt, *J. Chem. Phys.* **47** (1967) 1300.

[40] J. Gauss, *J. Chem. Phys.* **99** (1993) 3629.

[41] D.B. Chesnut, *Annu. Rep. NMR Spectrosc.* **29** (1994) 71.

[42] M. Kaupp, V.G. Malkin, O.L. Malkina and D.R. Salahub, *Chem. Phys. Lett.* **235** (1995) 382.

[43] R.A. Hegstrom, *Phy. Rev.* **A 19** (1979) 17.

[44] H. Le, J.G. Person, A.C. de Dios and E. Oldfield, *J. Am. Chem. Soc.* **117** (1995) 3800.

[45] W.H. Zachariasen, *Acta Crystallogr.* **A 31** (1975) 417.

[46] P.J. Hay and W.R. Wadt, *J. Chem. Phys.* **82** (1985) 270.

[47] M.J. Frisch, G.W. Trucks, H.B. Schlegel, G.E. Scuseria, M.A. Robb, J.R. Cheeseman, M.C. Strain, J.C. Burant, R.E. Stratmann, S. Dapprich, K.N. Kudin, J.M. Millam, A.D. Daniels, G.A. Petersson, J.A. Montgomery, V.G. Zakrzewski, K. Raghavachari, P.Y. Ayala, Q. Cui, K. Morokuma, J.B. Foresman, J. Cioslowski, J.V. Ortiz, V. Barone, B.B. Stefanov, G. Liu, A. Liashenko, P. Piskorz, W. Chen, M.W. Wong, J.L. Andres, E.S. Replogle, R. Gomperts, R.L. Martin, D.J. Fox, T. Keith, M.A. AlLaham, A. Nanayakkara, M. Challacombe, C.Y. Peng, J.P. Stewart, C. Gonzalez, M. Head-Gordon, P.M.W. Gill, B.G. Johnson and J.A. Pople, Gaussian98, Gaussian, Inc., (1998) Pittsburgh, PA.

[48] M.J.L. Sangster and M. Dixon, *Adv. Phys.* **25** (1976) 247.

[49] L. Verlet, *Phys. Rev.* **159** (1967) 98.

[50] N. Bloembergen, E.M. Purcell and R.V. Pound, *Phys. Rev.* **73** (1948) 679.

[51] R.E. Walstedt, R. Dupree, J.P. Remeika and A. Rodriguez, *Phys. Rev.* **B 15** (1977) 3442.

[52] P.I. Kuznetsov, R.L. Stratonovich and V.I. Tikhonov, *Theory Probab. its Appl.* **5** (1960) 80.

[53] P. Ewald, *Ann. Phys.* **64** (1921) 253.

[54] S.W. De Leeuw, J.W. Perram and E.R. Smith, *Proc. R. Soc. Lond.* **A 373** (1980) 27.

List of publications

1. *"Soft X-ray fluorescence measurements of irradiated polymer films"*
R. P. Winarski, D. L. Ederer, J. -C. Pivin, E. Z. Kurmaev, S. N. Shamin, A. Moewes, G. S. Chang, C. N. Whang, K. Endo and T. Ida, *Nucl. Inst. Meth.* **B 145** (1998) 401.

2. *"Structural analysis of $Ag_xCu_{1-x}I$ (0.75< x <1.00) in the superionic phase using solid ^{63}Cu NMR and X-ray diffraction methods"*
K. Endo, T. Ida, J. Kimura, M. Mizuno, M. Suhara and K. Kihara, *Chem. Phys. Lett.* **308** (1999) 390.

3. *"Analysis of ^{109}Ag MAS NMR chemical shieldings observed in $Ag_xCu_{1-x}I$ crystals"*
T. Ida, K. Endo, M. Suhara, M. Kenmotsu, K. Honda, S. Kitagawa and H. Kawabe, *Bull. Chem. Soc. Jpn.* **72** (1999) 2061

4. *"Radiation-induced degradation of polyethersulphone films studied by fluorescent X-ray emission spectroscopy"*
E. Z. Kurmaev, R. P. Winarski, K. Endo, T. Ida, A. Moewes, D. L. Ederer, J. -C. Pivin, S. N. Shamin, V. A. Trofimova and Yu. M. Yarmoshenko, *Nucl. Inst. Meth.* **B 155** (1999) 431.

5. *"A study of electron spin dynamics and phase transition in $[Co(H_2O)_6][SiF_6]$ by single crystal ^{19}F NMR spin-lattice relaxation time measurements"*
M. Mizuno, T. Ida, H. Nakahama and M. Suhara, *Phys. Chem. Chem. Phys.* **1** (1999) 4561.

6. *"X-ray fluorescence study of organic-inorganic polymer conversion into ceramics induced by ion irradiation"*
E. Z. Kurmaev, A. Moewes, M. Krietemeyer. K. Endo, T. Ida, S. Shimada, R. P. Winarski, M. Neumann, S. N. Shamin and D. L. Ederer, *Phys. Rev.* **B 60** (1999) 15 100.

7. *"Soft X-ray fluorescence measurements of polyimide films"*
R. P. Winarski, D. L. Ederer, E. Z. Kurmaev, S. N. Shamin, K. Endo, T. Ida, A. Moewes, G. S. Chang, S. Y. Kim and C. N. Whang, *Thin Solid Films* **357** (1999) 91.

8. *"Structure analysis of $Ag_xCu_{1-x}I$ ($0 \leq x \leq 0.5$) by solid ^{63}Cu NMR and X-ray diffraction methods"*
J. Kimura, T. Ida, M. Mizuno, K. Endo, M. Suhara and K. Kihara, *J. Mol. Struct.* **522** (2000) 61.

9. *"Analysis of incommensurate structure in $[N(CH_3)_4]_2ZnCl_4$ crystal"*
T. Ida, M. Mizuno and M. Suhara, *Phase Transitions* **72** (2000) 43.

10. *"Chemical reactions in polymers induced by ionbeam mixing: Fluorescence X-ray measurements"*
E.Z. Kurmaev, R.P. Winarski, J.-C. Pivin, D.L. Ederer, S.N. Shamin, A. Moewes, K. Endo, T.Ida, G.S. Chang and C.N. Wang, *J. Elec. Spec. Rel. Phen.* **110-111**

(2000) 87.

11. *"Theoretical X-ray photoelectron and emission spectra of C-, N- and O- containing polymers by density-functional theory calculations using model molecules"*
S. Shimada, T. Ida, K. Endo, M. Suhara, E.Z. Kurmaev and D.P. Chong, *Polymer Journal* **32** (2000) 12.

12. *"Theoretical X-ray photoelectron and emission spectra of Si- and S-containing Polymers by density-functional calculations using model molecules"*
K. Endo, S. Shimada, T. Ida, M. Suhara, E.Z. Kurmaev, A. Moewes and D.P. Chong, *J. Mol. Struct.* in press.